How to determine precisely luminosity at pp machine (LHC) ?

15.10.2021

Krzysztof Doroba

Based on: Precision luminosity measurements in proton-proton collision at $\sqrt{s}$ = 13TeV in 2015 and 2016 at CMS,
The CMS Collaboration, arXiv:2104.01927v2, Eur. Phys. J. C81 (2021)800

Outline of the talk:

- Short introduction
- Luminometers and algorithms used
- Van der Meer's and other scans results
- Systematic error determination
- How to do physics without knowledge of luminosity? (TOTEM)

LHC BEAM STRUCTURE:

$$f_{RF} = h * \nu_r;$$

f_{RF} - $RF\ frequency$; ν_r $-$ $circulation\ rate$; h $-$ $harmonic\ number$

@LHC $f_{RF} = 400\ MHz;$ ν_r = c/26659 m ; $\rightarrow h = 35640$

RF@LHC system has 35640 "RF BUCKETS"

In each RF bucket proton bunch may be located, but
if all RF buckets would be occupied then

- Time distance between bunches would be 2.5 ns
- Somehow such a sequence of bunches should be delivered to LHC
- Power / power dissipation?

So only one in ten RF BUCKED contains PROTON BUNCH

- minus steering bunches; this gives 2808 bunches max for physics

This is PS which decides about beam structure

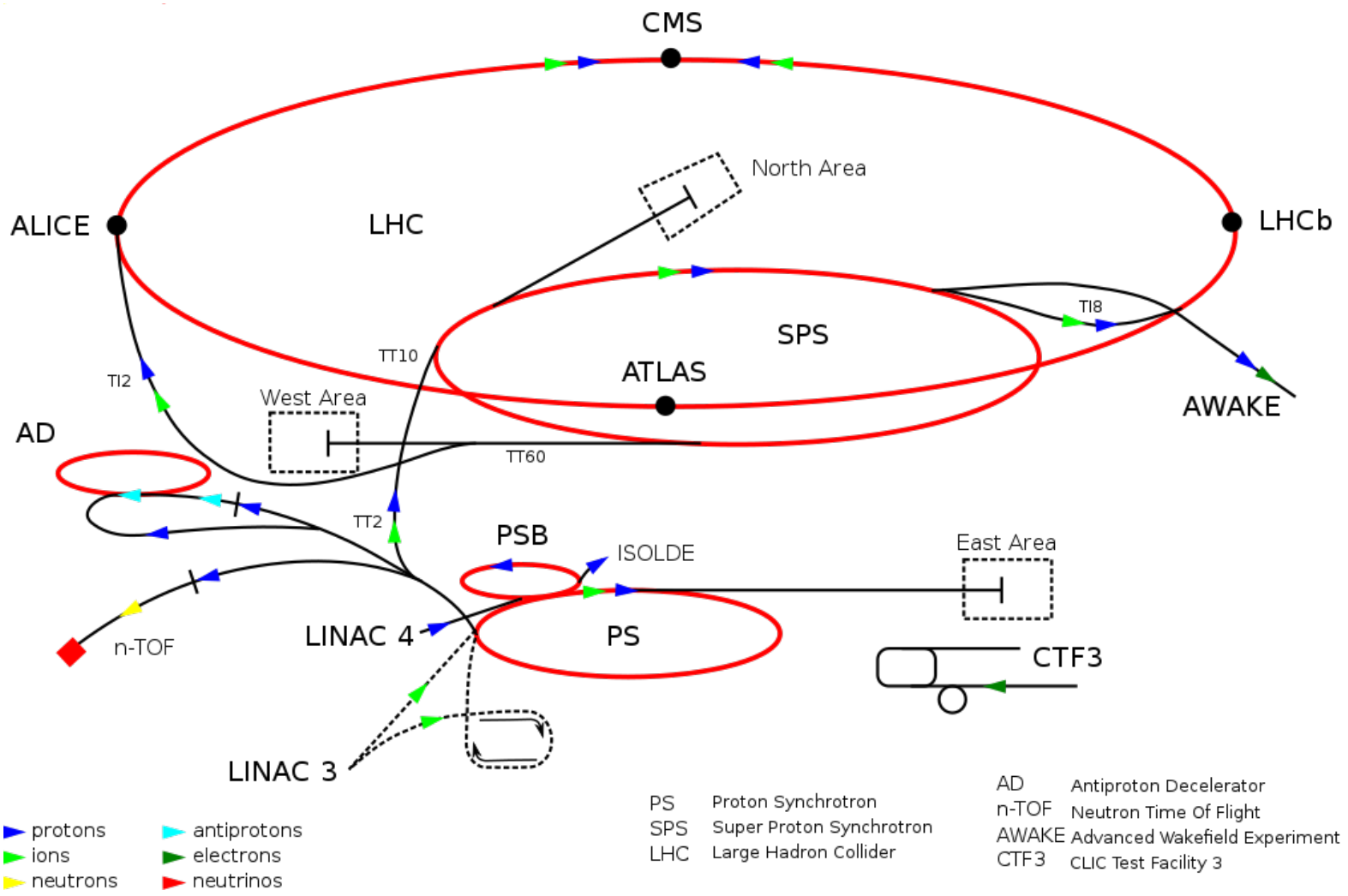
CMS
North Area
ALICE
LHC
LHCb
SPS
TI8
TT10
ATLAS
TI2
West Area
AWAKE
AD
TT60
TT2
PSB
ISOLDE
East Area
n-TOF
LINAC 4
PS
CTF3
LINAC 3
protons
ions
neutrons
antiprotons
electrons
neutrinos
PS Proton Synchrotron
SPS Super Proton Synchrotron
LHC Large Hadron Collider
AD Antiproton Decelerator
n-TOF Neutron Time Of Flight
AWAKE Advanced Wakefield Experiment
CTF3 CLIC Test Facility 3

intensity [155, 156]. For the LHC beam each PSB bunch has an intensity of some $1.6 \cdot 10^{12}$ protons, slightly more than twelve times the intensity of an LHC bunch because of losses during transfer and capture in the PS. The transfer between the four rings of the PSB and the PS is sketched in Fig. 5.2. During the first transfer, bunches from all four booster rings are stringed

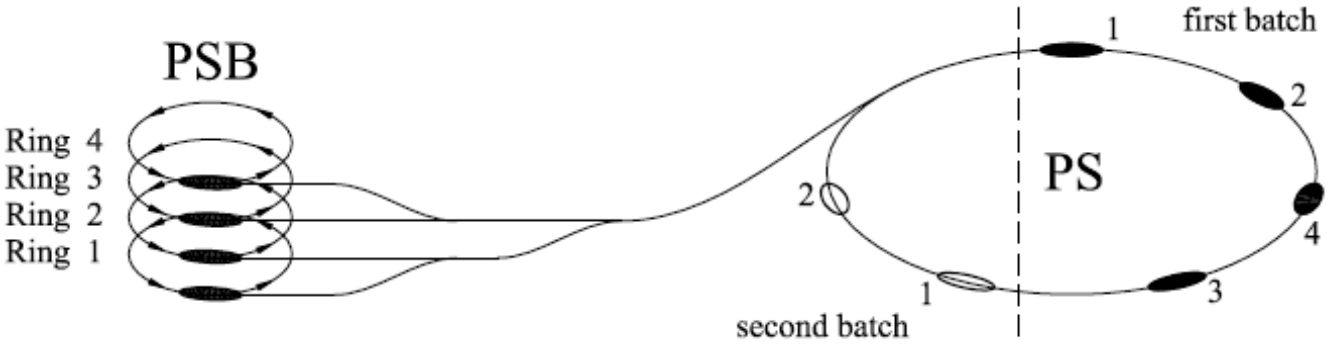

Fig 5 2: Double batch transfer scheme from PSB to PS. For the injection into the PS all four booster rings are used, each delivering one bunch. The second injection is performed with two booster bunches only.

up in the PS. One PSB machine cycle later (corresponding to 1.2 s), half of the rings are used to deliver two more bunches. Finally, six of seven PS buckets are populated. The empty bucket is needed for the transfer from the PS to the SPS to preserve a gap for the beam ejection.

final energy would be some 300 ns, and the longitudinal emittance would be much too large to capture these bunches in the SPS. Therefore each bunch is split into twelve equal fractions, which reduces the longitudinal emittance per bunch to a value that is acceptable for the SPS. The bunch spacing is also divided by twelve to the nominal LHC parameter of 25 ns. The splitting factor can be decomposed to $12 = 3 \cdot 2 \cdot 2$, so that one triple-splitting and two bunch pair splittings are performed (see Sec. 3.2.2). To keep the RF frequencies during acceleration within the capabilities of the main RF system in the PS (2.8 to 10 MHz) [161, 162], the triple splitting is initiated during the injection flat-bottom at 1.4 GeV [163]. Thereafter the beam is accelerated on $h = 21$ and subsequently the bunches are split twice to $h = 42$ and finally to $h = 84$. The RF gymnastics for the preparation of the LHC beam in the PS is illustrated in Fig. 5.3. Finally one ends with a batch of 72 bunches and, as the empty bucket splits exactly

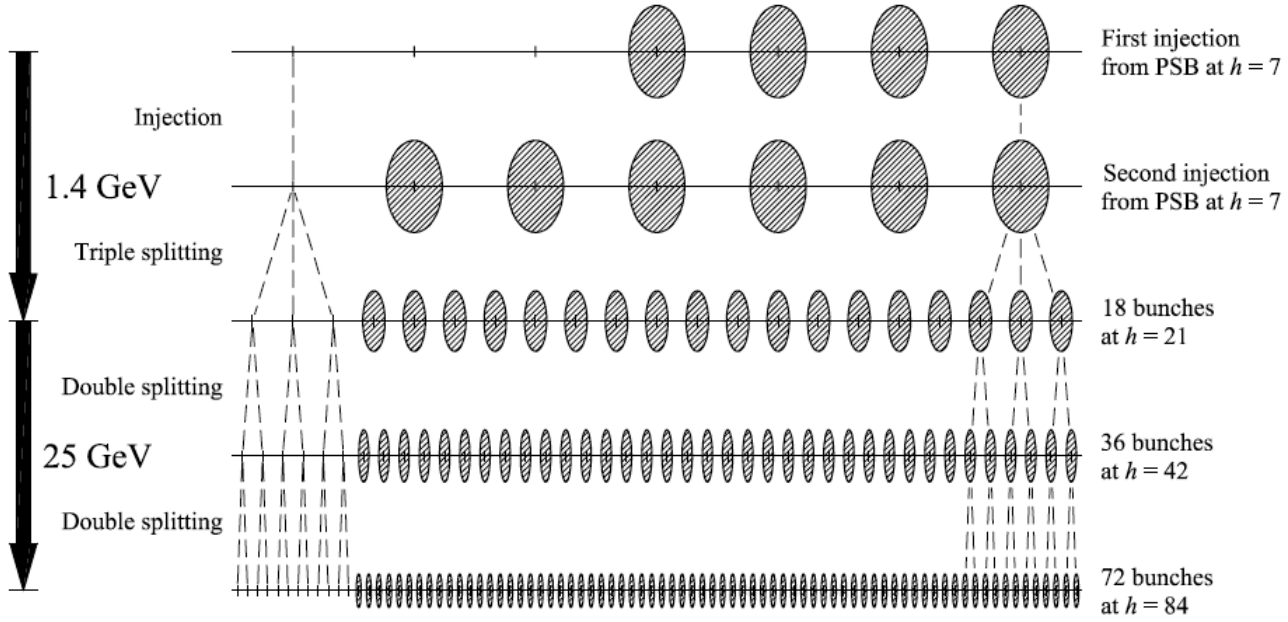

Fig 5 3: Acceleration and bunch splitting scheme of the nominal LHC beam in the PS. Starting from $4 + 2$ bunches from the PSB each of them is split twelve times in total so that on ends up with a batch of 72 bunches at $h = 84$ with 25 ns. The empty bucket is also multiplied, and the gap is therefore 12 bunch positions long.

Luminosity $\mathcal{L}$: (absolute luminosity)

per bunch crossing

$$\mathcal{L}_b = \nu_r n_1 n_2 K \int \varrho_1(x,y,z,t)\varrho_2(x,y,z,t)dxdydzdt$$

K – kinematic factor

$$\mathcal{L} = \sum_b \mathcal{L}_b$$

Sum over all colliding bunches

☹

For head on collisions:

$$\mathcal{L}_b = \nu_r n_1 n_2 2c \int \varrho_1 \varrho_2 dxdydzdt = \frac{\nu_r n_1 n_2}{2\pi\Sigma_x\Sigma_y}$$

n_j --number of protons inside bunch, ν_r -circulation rate

$$\Sigma_j = \sqrt{\sigma_{j1}^2 + \sigma_{j2}^2};$$

For $\sigma_{j1} = \sigma_{j2}$

$$\mathcal{L}_b = \frac{\nu_r n_1 n_2}{4\pi\sigma_1\sigma_2}$$

σ_{jn}, σ_j – dispersions

Some well know $\mathcal{L}$ measurements:

ISR (pp DC machine, max 57 A per ring,) , max $\mathcal{L} = 1.4 * 10^{32}\ cm^{-2}s^{-1}$

min $\frac{\Delta\mathcal{L}}{\mathcal{L}} \sim 1\%$, $\mathcal{L}$ *measurement* : van der Meer's scan (vertical only!)

$$\mathcal{L} = \frac{I_1 I_2}{e^2 c * tan(\alpha)} * \frac{1}{h_{eff}} \qquad h_{eff} = \frac{1}{\int \rho_{z1}(z)\rho_{z2}(z)dz}$$ ☺

LEP (e^+e^- machine, max 6.2 mA per ring,) , max $\mathcal{L} = 1.0 * 10^{32}\ cm^{-2}s^{-1}$

min $\frac{\Delta\mathcal{L}}{\mathcal{L}} \sim 0.1\%$, $\mathcal{L}$ measurement: Bhabha scattering (+scan vdM)

$$\mathcal{L} = {}^{R}/_{\sigma}\ [cm^{-2}s^{-1}],$$ *R - reaction frequency*

σ *– cross section*

This formula works not only for Bhabha scattering

In the formula $\mathcal{L} = {}^{R}/_{\sigma}\ [cm^{-2}s^{-1}]$ σ may refer to:

- Elastic cross section
- Total cross section (optical theorem) (TOTEM)
- W and Z production
- … (depending on precision of the predictions) ☺

The LHC beam has a structure (bunches), number of interaction per bunch xing is large and fluctuates (Poisson), so:

- Luminometers has to be linear in the wide range.
- Luminosity has to be measured separately for each bunch xing

$$\mathcal{L} = \sum_{b} \mathcal{L}_b$$

Sum is over all colliding bunches

- for good knowledge of the systematic error different luminometers as well as different schemes of luminosity determination have to be used
- Precise knowledge of luminosity is profitable:

$$\frac{\delta m_t}{m_t} \sim \frac{\delta \sigma}{\sigma}$$

$$\sigma_Z, \sigma_W\ (theory)\ depends\ on\ PDF \rightarrow\ PDF\ choice$$

All possible SM precision tests, UPC, ...

Which devices are used at CMS for luminosity measurement?

- Pixel Cluster Counting - PCC
- Primary Vertex Counting - PVC
- Hadron Forward Occupancy Counting - HFOC
- Pixel Luminosity Telescope - PLT
- Fast Beam Condition Monitor - FBCM/BCM1F, 6.2 ns resolution, 1.8 m from xing; distinguish lumi from beam-gas
- DT (drift tubes for muon system, integrated over bunches)
- Single Bunch Response - SBR
- Radiation Monitoring System for Environment and Safety - RAMSES ionization chambers at atm. pressure (integrated)
- Beam Position Monitor - BPM (at DOROS-Diamond ORbit and OScillation or at LHC arcs)
- Beam Imaging Method - BIM (by LHCb, based on beam-gas int.)
- Beam Pick-up Timing for eXperiments - +-175 m BPTX
- Bunch Crossing IDentifier - BCID
- Longitudinal Density Monitors - LDM
- Fast Beam Current Transformer -FBCT
- Direct Current Beam Transformer - DCCT

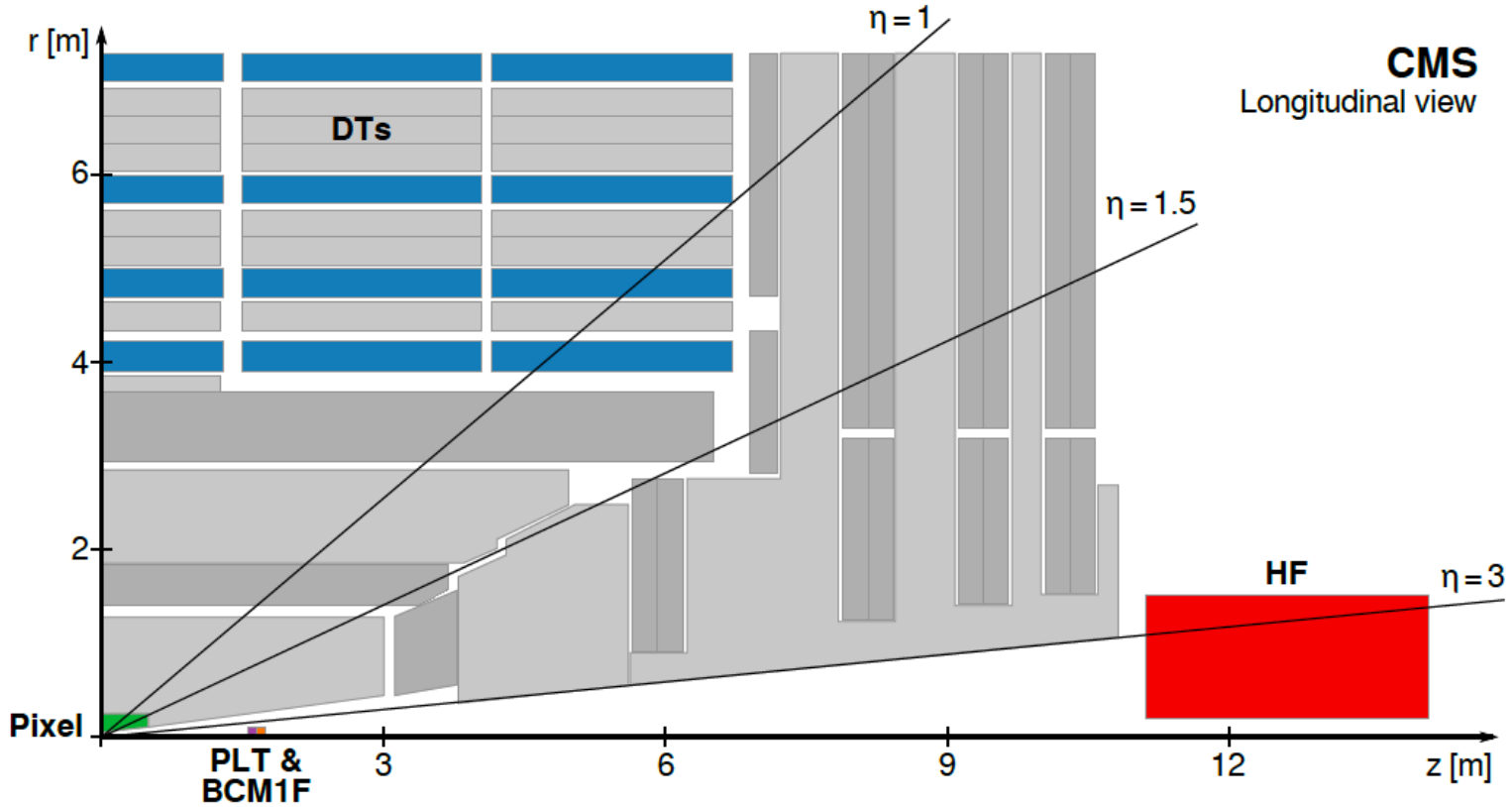

Figure 1: Schematic cross section through the CMS detector in the *r*-*z* plane. The main luminometers in Run 2, as described in the text, are highlighted, showing the silicon pixel detector, PLT, BCM1F, DTs, and HF. The two RAMSES monitors used as a luminometer in Run 2 are located directly behind HF. In this view, the detector is symmetric about the horizontal and vertical axes, so only one quarter is shown here. The center of the detector, corresponding to the approximate position of the pp collision point, is located at the origin. Solid lines represent distinct η values.

Separate DAQ for HF, PLT, BCM1F +LHC beam related data

Luminometers:

- Piksel Claster Counting (PCC)

  $2 * 10^7$ pixels guarantees good linearity even for high μ

Monte Carlo !!!

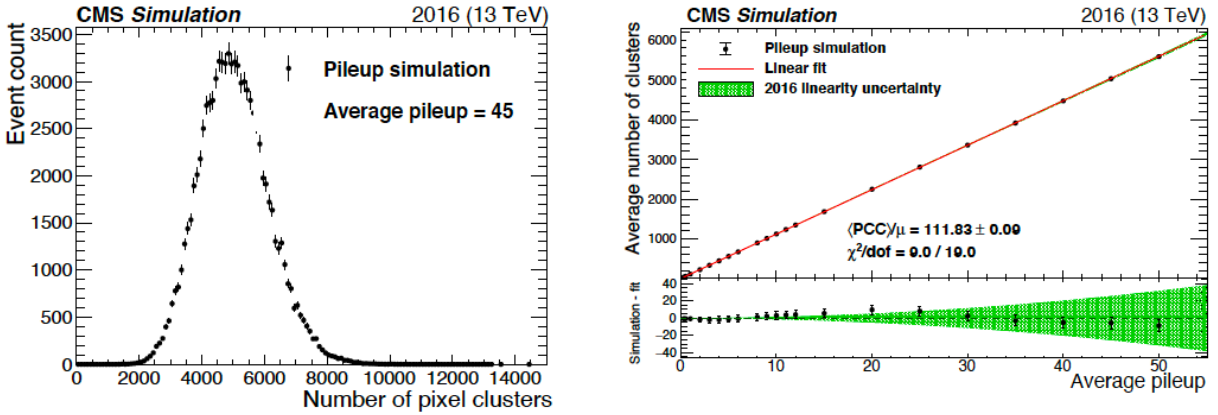

Figure 2: The left plot shows the number of pixel clusters and their statistical uncertainty from simulation of pileup following a Poisson distribution with a mean of 45. The right plot shows the mean number of pixel clusters from simulation as a function of mean pileup. The red curve is a first-order polynomial fit with slope and χ^2/dof values shown in the legend. Only pixel modules considered for the PCC measurement in data are included. The lower panel of the right plot shows the difference between the simulation and the linear fit in black points. The green band is the final linearity uncertainty for the 2016 data set.

$\mu = 27$ in 2016

Luminometers (continued):

- Primary vertex counting (PVC)
  vertexes with min 11 tracks. Methods fails for large μ.
  good for vdM method as a crosscheck
- HFOC – FPGA guarantees independent readout (40 MHz) for lumi measurement (# ADC channels over threshold).
- Pixel Luminosity Telescope (PLT) 48 sensors located in 8+8 telescopes. Triple coincidence required.
- Fast Beam Condition Monitor FBCM/BCM1F.
  1.8 m from xing, 6.25 ns time resolution, diamond crystals separate beam-gas interactions from those coming from xing.
- DT data from muon track finder. Low rate, sum over all bunches.

- Luminometers cd:
- RAdiation Monitoring System for the Environment and Safety
  RAMSES – like DT sum over all bunches

Algorithmuses for luminosity determination:

- $< N_{observables} > = < N_{observables/interaction} >< N_{interaction} >$
  $\equiv < N_{observables/interaction} > \mu$

  average # observables: (hits, tracks, clusters….)

  μ – average # interactions per bunch xing (all)

  (average over (short) period of time)

to determine instantaneous LHC luminosity we use formula

$$\mu = \frac{\sigma \mathcal{L}_b}{\nu_r}$$

$where: \quad \nu_r = 11245.6\, kHz\,, \sigma - total\ cross\ section;$

Algorytm rate-scaling: (for PCC, PVC, DT, RAMSES)

$$\mathcal{L}_b = \frac{< N_{observables} >}{< N_{observables/interaction} >} * \frac{\nu_r}{\sigma} = < N_{observables} > \frac{\nu_r}{\sigma_{vis}}$$

Algorithm zero counting: (HFOC, PLT, BCM1F)

Assuming that the probability of no observables in a single collision is p, then the probability of no observables seen in a bunch crossing with k interactions is thus simply p^k. Averaged over a large number of bunch crossings, with the number of interactions per bunch crossing distributed according to a Poisson distribution of mean μ, the expected fraction of events with zero observables recorded, $\langle f_0 \rangle$, can be expressed as:

$$\langle f_0 \rangle = \sum_{k=0}^{\infty} \frac{\mathrm{e}^{-\mu}\mu^k}{k!} p^k = \mathrm{e}^{-\mu(1-p)}. \tag{5}$$

$$\mathcal{L}_\mathrm{b} = \mu \frac{\nu_r}{\sigma} = -\ln \langle f_0 \rangle \frac{1}{1-p} \frac{\nu_r}{\sigma} \equiv -\ln \langle f_0 \rangle \frac{\nu_r}{\sigma_\mathrm{vis}}.$$

Absolute luminosity calibration

Each luminometer has to be calibrated!!!!

How to do it ?

- On the basis of theoretical calculations and Monte Carlo but for LHC expected accuracy far from 1%
- With van der Meer method (moving both beams by constant step in opposite directions)
- Beam Imaging Method – LHCb : single beam, beam – gas
- Other auxiliary scanning (Beam Imaging, Length Scale Calibration)

Beams in van der Meer (vdM) method: 0 crossing angle, ~30 bunches, (8-9)x10^{10} protons each, $\mu \approx 0.6$, $\sigma_b = 100\ \mu m$, optics $\beta^* \approx 19\ m$

AIM: determine Σ_x, Σ_y from fits to luminometer rates during scan→ $\mathcal{L}_b = \frac{\nu_r n_1 n_2}{2\pi \Sigma_x \Sigma_y}$

$$\sigma_{vis} = \frac{\mu_{vis}}{\mathcal{L}_b}$$

3 scannings performed (and used) for 13 TeV beams (2015, 2016)

For each vdM scan: 2x25 ↑↓ steps, 30 seconds each, up to distance $6\sigma_b$ and back

Beam position measurement: DOROS BPM, LHC arc BPM

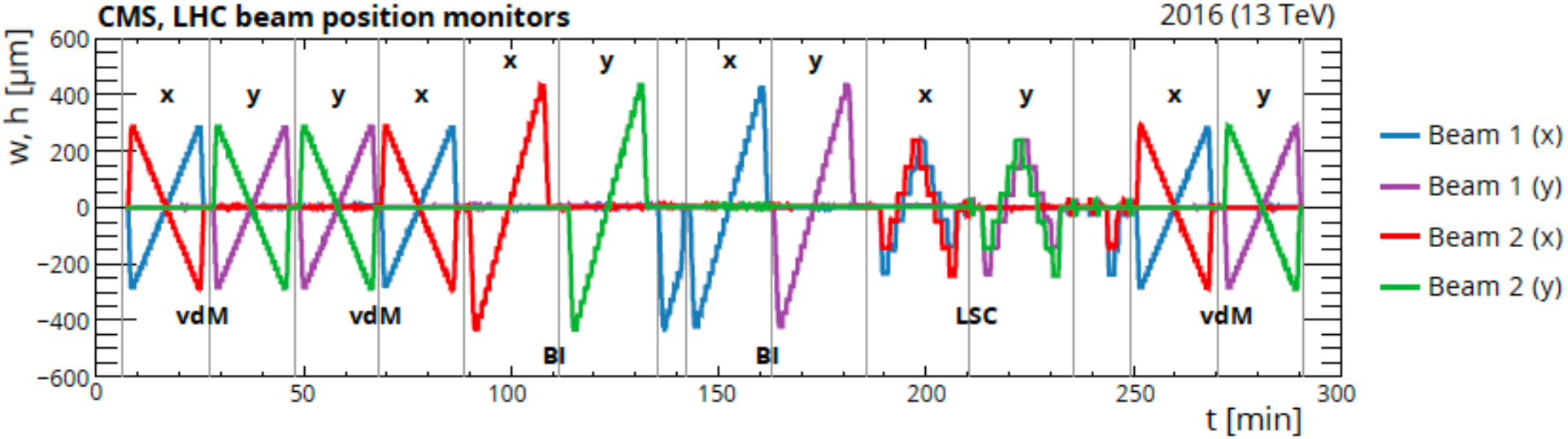

Figure 3: Relative change in the positions of beams 1 and 2 measured by the DOROS BPMs during fill 4954 in the horizontal (x) or vertical (y) directions, as a function of the time elapsed from the beginning of the program. The gray vertical lines delineate vdM, BI, or LSC scans.

Equations (11) and (12) are quite general, and do not depend on the assumption of Gaussian-distributed bunches. Indeed, it is frequently the case that simple Gaussians do not provide an adequate description of the scan-curve data. In such cases, we use double-Gaussian functions of the form

$$f(x) = \frac{1}{\sqrt{2\pi}}\left[\frac{\epsilon_x}{\sigma_{1x}}\exp\left(-\frac{x^2}{2\sigma_{1x}^2}\right) + \frac{1-\epsilon_x}{\sigma_{2x}}\exp\left(-\frac{x^2}{2\sigma_{2x}^2}\right)\right], \tag{14}$$

where ϵ_x is the fraction of the Gaussian with width σ_{1x}. Normally the Gaussian with the smaller width σ_{1x} is considered the core Gaussian, while the Gaussian with the larger width σ_{2x} is used to fit the tails of the scan curve. Similar relations apply for the y coordinate. The effective value of Σ_i $(i = x, y)$ is then given by

$$\Sigma_i = \frac{\sigma_{1i}\,\sigma_{2i}}{\epsilon_i\sigma_{2i} + (1-\epsilon_i)\sigma_{1i}}. \tag{15}$$

To calibrate a given luminosity algorithm, the absolute luminosity computed from beam parameters via Eq. (13) is used in conjunction with Eq. (3) to obtain

$$\sigma_{\text{vis}} = \mu_{\text{vis}}\frac{2\pi\Sigma_x\Sigma_y}{n_1 n_2}, \tag{16}$$

where μ_{vis} is the visible interaction rate. In this analysis, μ_{vis} is taken as the arithmetic mean of the peak values from $\mathcal{L}(w,0)$ and $\mathcal{L}(0,h)$ in scans that are performed sufficiently close in time

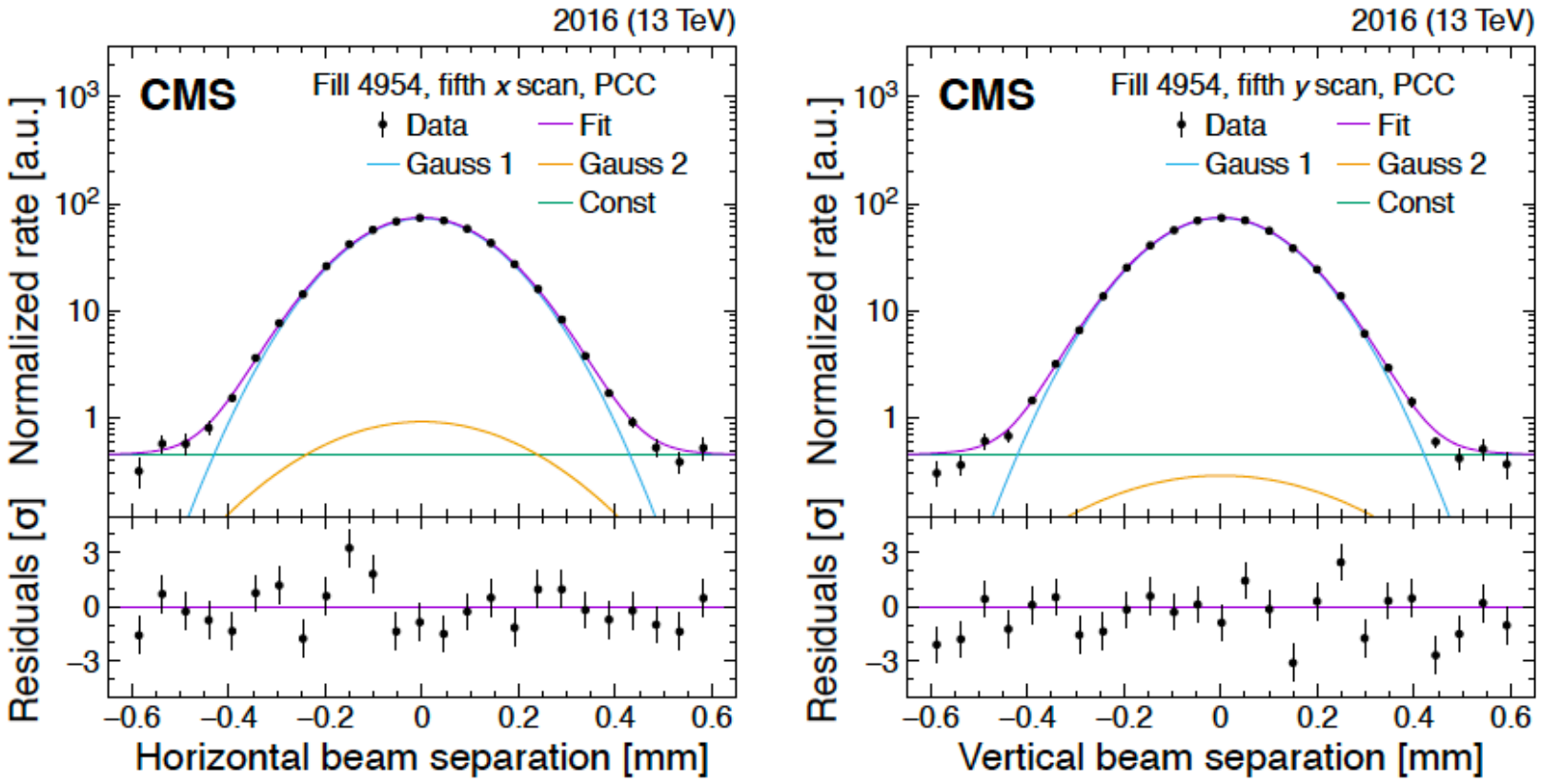

Figure 4: Example vdM scans for PCC for BCID 41, from the last scan pair in fill 4954, showing the rate normalized by the product of beam currents and its statistical uncertainty as a function of the beam separation in the x (left) and y (right) direction, and the fitted curves. The purple curve shows the overall double-Gaussian fit, while the blue, yellow, and green curves show the first and second Gaussian components and the constant component, respectively. All corrections described in Section 4.3 are applied. The lower panels display the difference between the measured and fitted values divided by the statistical uncertainty.

A_{eff} - effective area of beam crossing obtained in vdM scan

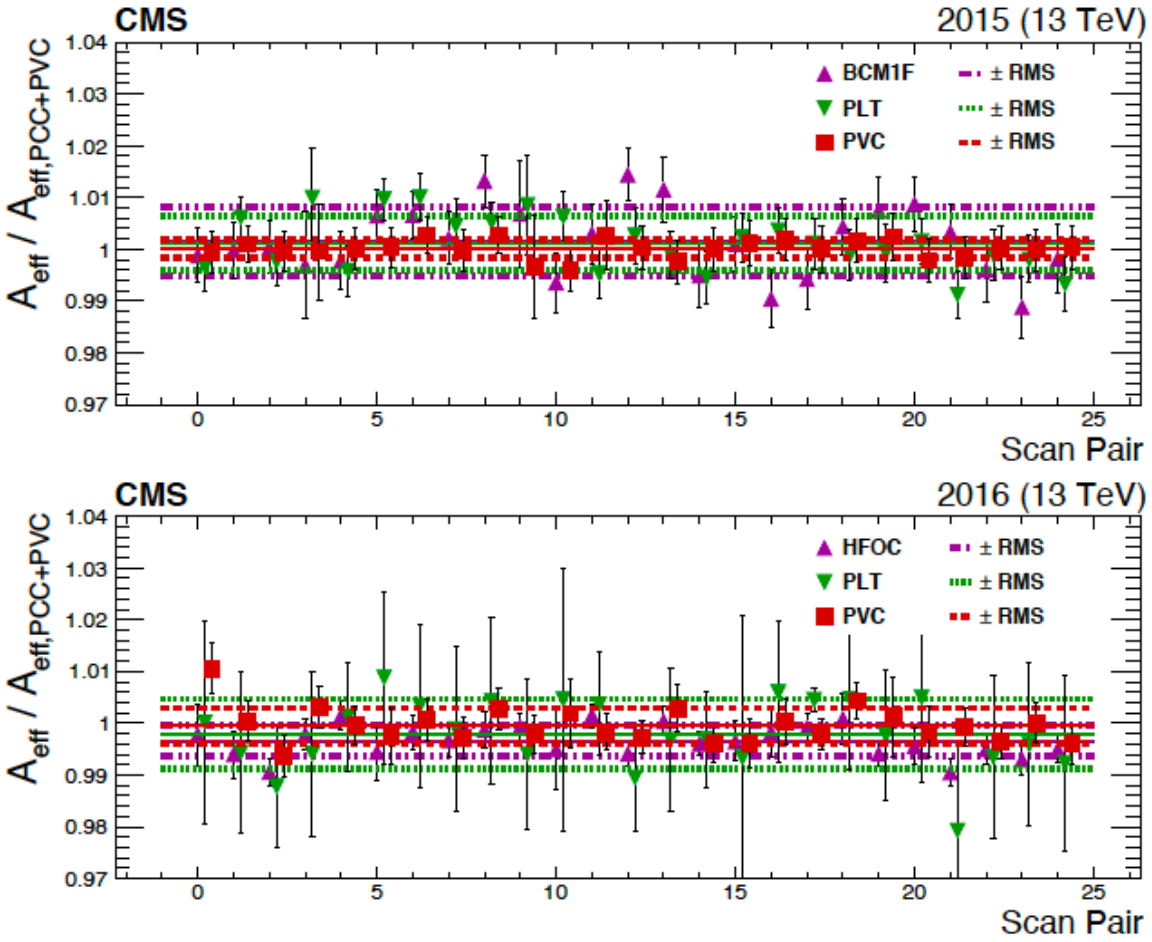

Figure 5: The two figures above show comparisons of effective area (A_{eff}) of cross-check luminometers with respect to the nominal PCC+PVC for fills 4266 (upper) and 4954 (lower). The points are the ratio of the A_{eff} of the labeled luminometer to PCC+PVC. There are 25 A_{eff} values because there are five scan pairs with five BCIDs analyzed for each scan pair. The solid lines are the average of all the A_{eff} while the bands are the standard deviations. In both sets of data the average comparison is compatible with unity within or near the standard deviation.

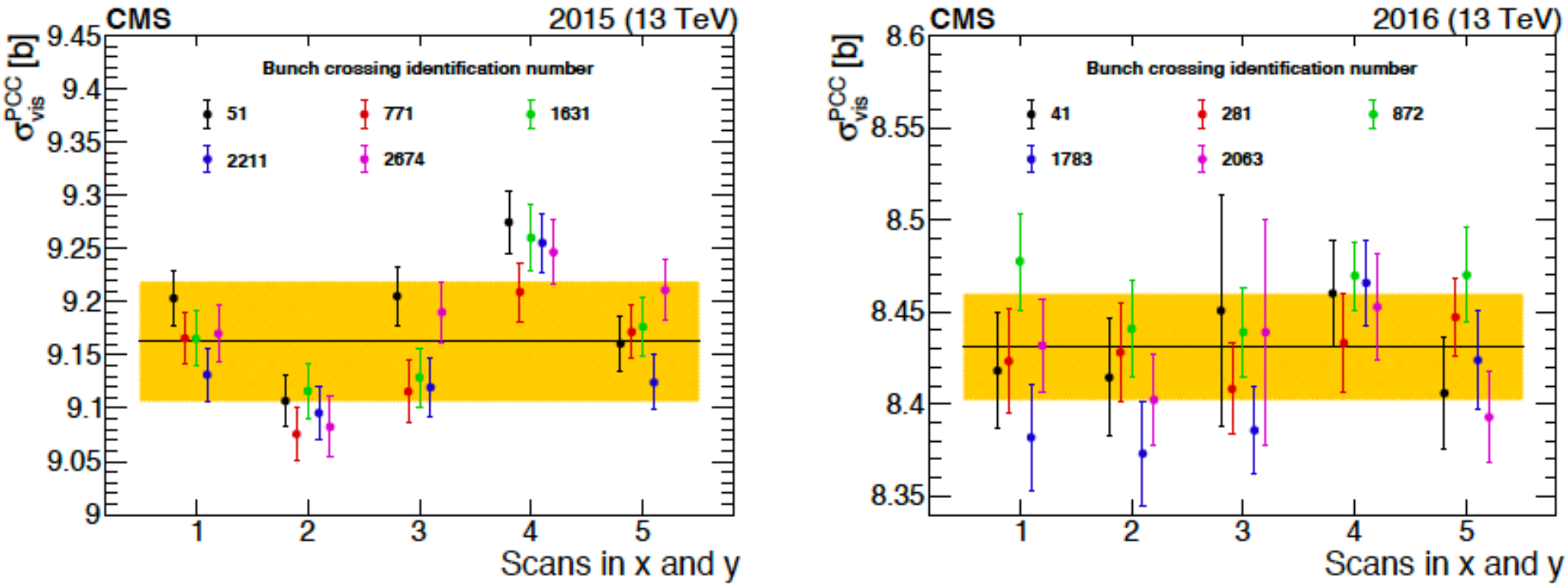

Figure 5: The measured $\sigma_{\text{vis}}^{\text{PCC}}$, corrected for all the effects described in Section 4.3, shown chronologically for all vdM scan pairs (where 3 and 4 are BI scans) taken in fills 4266 (left) and 4954 (right), respectively. Each of the five colliding bunch pairs is marked with a different color. The error bars correspond to the statistical uncertainty propagated from the vdM fit to $\sigma_{\text{vis}}^{\text{PCC}}$. The band is the standard deviation of all fitted $\sigma_{\text{vis}}^{\text{PCC}}$ values.

Systematic effects influencing σ_{vis} measurements

- Charge outside bunches

  (*ghost* – charge in neighboring RF buckets (measured by DCCT, FBCT)

  spurious –charge in steering bunches (measured by LHC LDM))

- Beam orbit displacement

  - orbit flow (DOROS, arc BPM vs nominal position LHC)
  - random orbit changes (single beam measurement)
  - difference between CMS vtx measurement and expected position according to dipole current (LSC)

- Beam – beam interaction (β^*, beam deviation)

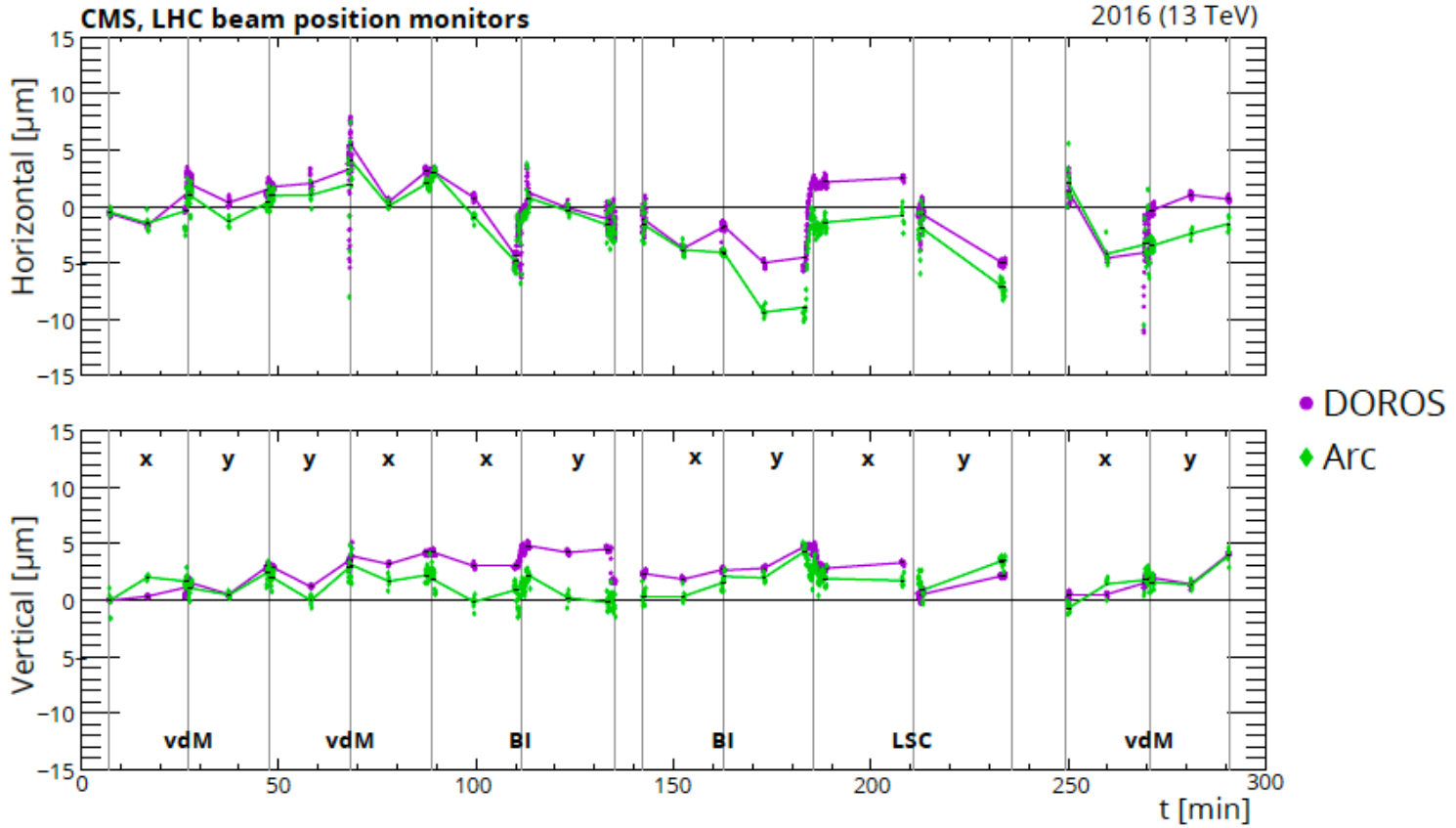

Figure 6: Effect of orbit drift in the horizontal (upper) and vertical (lower) beam-separation directions during fill 4954. The dots correspond to the beam positions measured by the DOROS or LHC arc BPMs in μm at times when the beams nominally collide head-on and in three periods per scan (before, during, and after) represented by the vertical lines. First-order polynomial fits are subsequently made to the input from BPMs (dots) and are used to estimate the orbit drift at each scan step. Slow, linear orbit drifts are corrected exactly in this manner, and more discrete discontinuities are corrected on average.

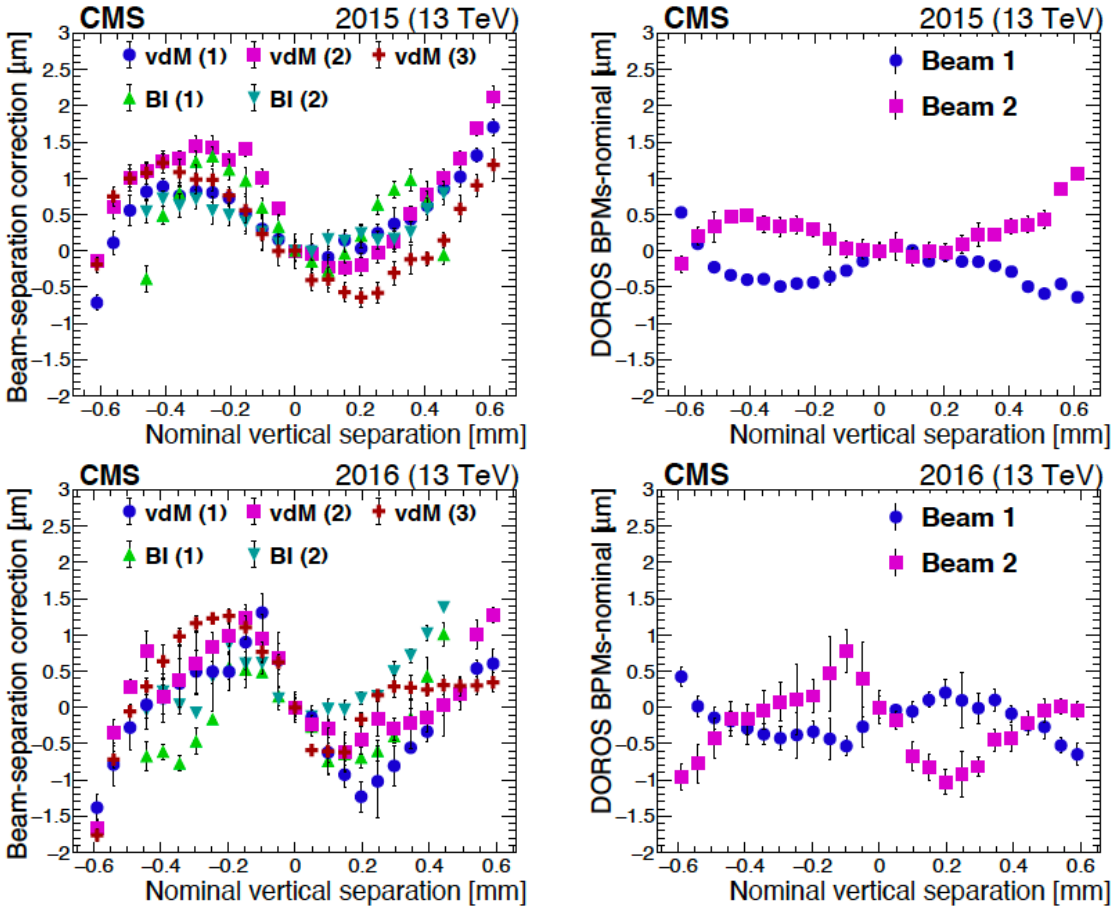

Figure 7: The beam-separation residuals in y during all scans in fills 4266 (upper) and 4954 (lower) are shown on the left. The dots correspond to the difference (in terms of beam separation in μm) between the corrected beam positions measured by the DOROS BPMs and the beam separation provided by LHC magnets ("nominal"). The error bars denote the standard deviation in the measurements. The figures on the right show the residual position differences per beam between the DOROS BPMs and LHC positions for the first vdM scans in y in fills 4266 (upper) and 4954 (lower).

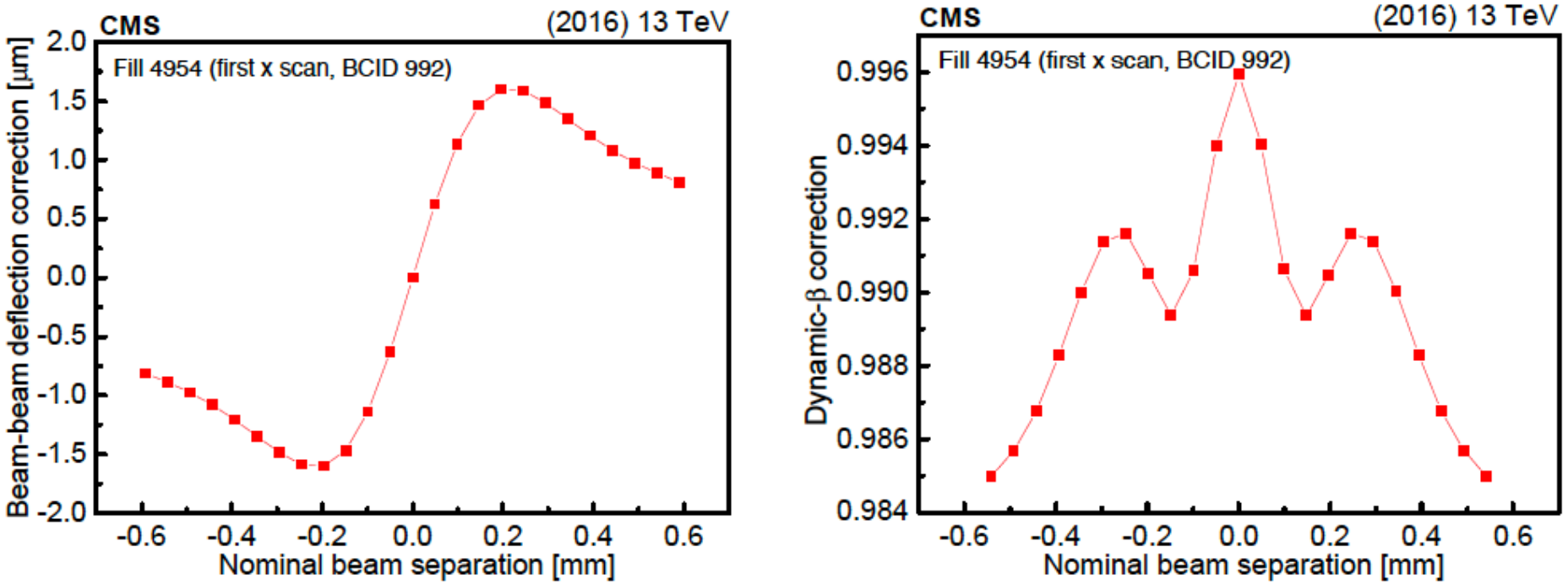

Figure 8: Calculated beam-beam deflection due to closed-orbit shift (left) and the multiplicative rate correction for PLT due to the dynamic-β effect (right) as a function of the nominal beam separation for the beam parameters associated with fill 4954 (first scan, BCID 992). Lines represent first-order polynomial interpolations between any two adjacent values.

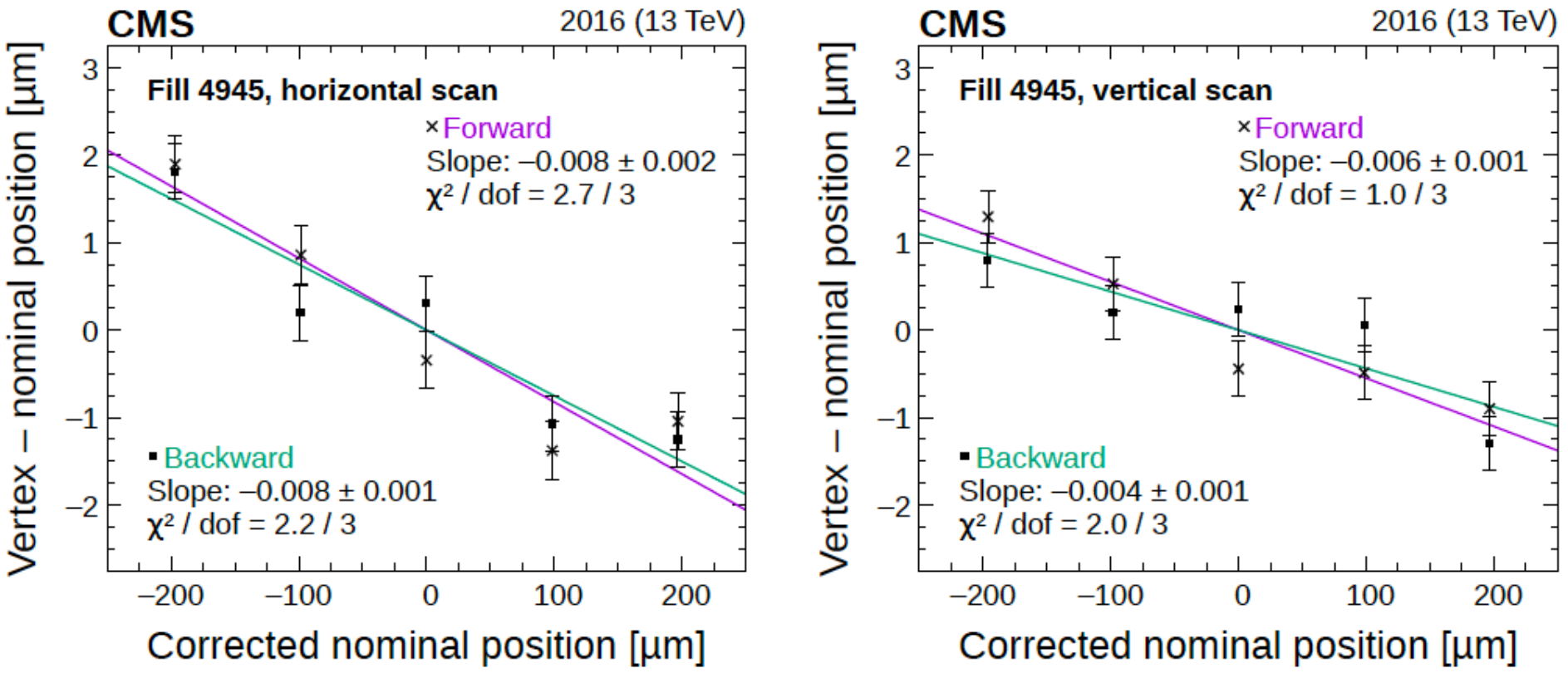

Figure 9: Fits to LSC forward (purple) and backward (green) scan data for the x (left) and y (right) LSC scans in fill 4945. The error bars denote the statistical uncertainty in the fitted luminous region centroid.

Beam density distribution -factorization?

Beam Imaging scanning BI

(only one beam is being shifted in x and y)

The best description of the BI data collected in 2015 and 2016 for the five bunch crossings used is achieved consistently with a sum of three Gaussian distributions, where the narrow component has a negative weight:

$$\rho_j(x,y) = -w_{j,1}g_{j,1}(x,y) + w_{j,2}g_{j,2}(x,y) + (1 + w_{j,1} - w_{j,2})g_{j,3}(x,y). \quad (22)$$

Figure 10 shows the two-dimensional pull distribution, i.e., $(N^{\text{vtx}}_{\text{data}} - N^{\text{vtx}}_{\text{fit}})/\sigma_{\text{data}}$, and the one-dimensional projections for the vertex distributions collected in the BI scan where the first beam is moved vertically for one bunch crossing in fill 4954. In these fits, the effects from the beam-beam deflection and dynamic-β are included in the positions of the reconstructed vertices and as per-vertex weights, respectively, whereas the impact of orbit drift is negligibly small.

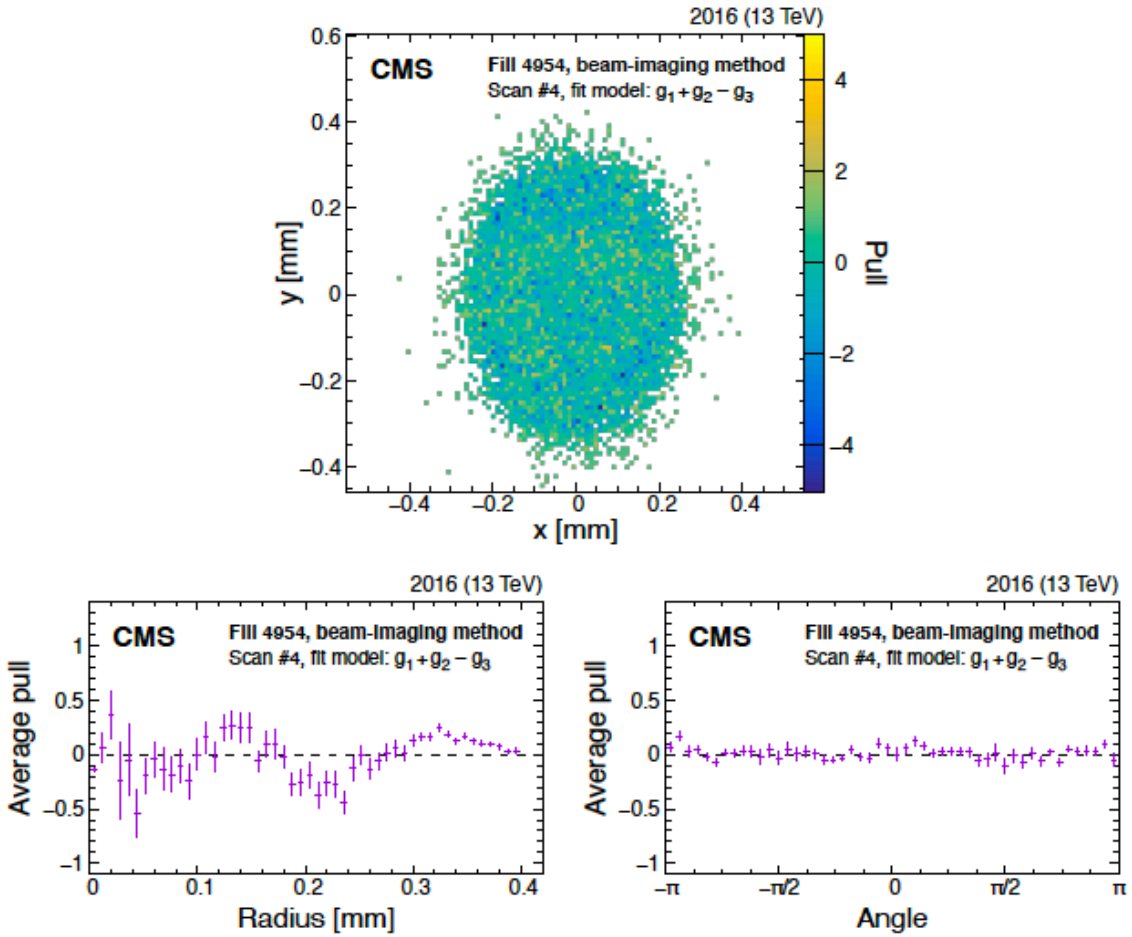

Figure 10: Example of the pull distributions of the fit model of Eq. (22) with respect to the vertex distribution that constrains beam 2 in the y direction recorded in fill 4954. The upper plot shows the two-dimensional pull distributions, and the lower plots show the per-bin pulls averaged over the same radial distance (lower left) or angle (lower right). The error bars in the lower plot denote the standard error in the mean of the pulls in each bin. The fluctuations observed in the radial projection of the residuals are included in the uncertainty estimation.

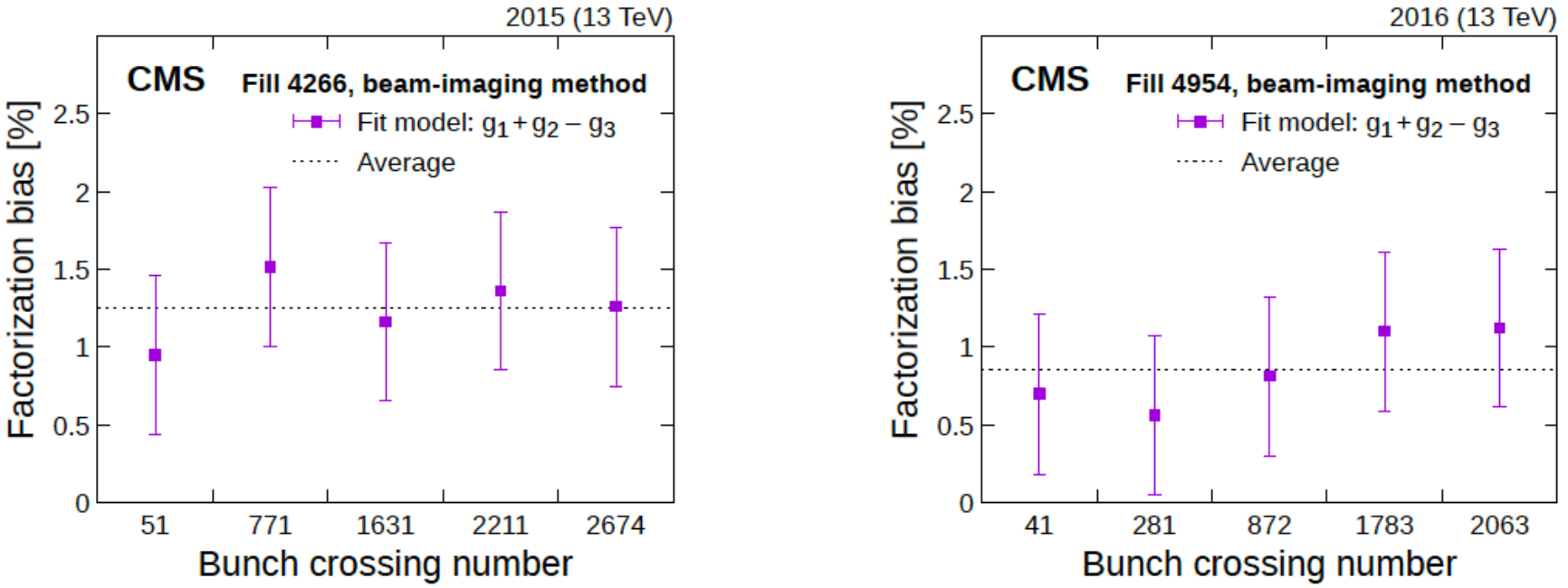

Figure 11: Factorization bias estimated from the fits to the BI bunch-by-bunch data in fills 4266 (left) and 4954 (right). The error bars denote sources of uncertainty (statistical and systematic), added in quadrature, in the factorization bias estimates.

Corrections coming from different interaction frequency for vdM and data taking

- Electronics connected (T1 - spillover, pedestal)
- Detectors material connected (T2 - afterglow)

$$\mathcal{L}_{b,corr}(n+1) = \mathcal{L}_{b,uncorr}(n+1) - \alpha_{T1}\mathcal{L}_{b,corr}(n)$$

$$\alpha_{T1} \simeq 0.005\ for\ BCM1F\ -0.09\ for\ PCC$$

T2 - influences all bunches.

correction: single or double exponential factor

small correction for vdM,

for full filling schemes 4(15)% for PCC (HFOC)

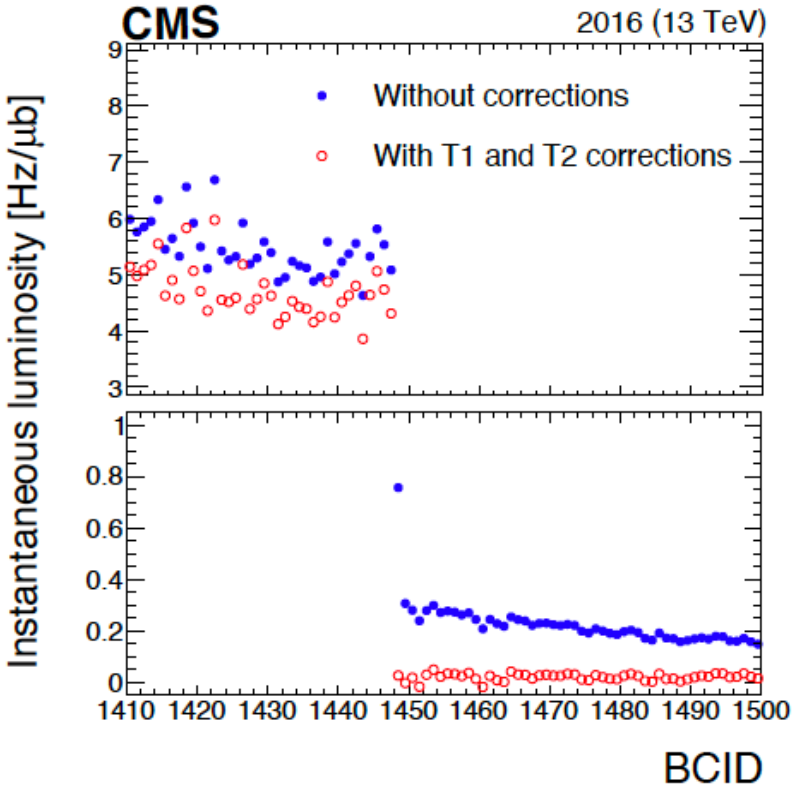

Figure 14: The instantaneous luminosity measured from PCC as a function of BCID before (filled blue points) and after (open red points) afterglow corrections are applied for each colliding bunch. The upper panel shows a subset of bunch crossings colliding at IP 5, and the lower panel shows empty bunch crossings (the scale is different in the two panels to show differences more clearly). The open red points in the lower panel lie close to 0, indicating that any residual PCC response is small in empty bunch slots.

Time stability

- (different pixels area)

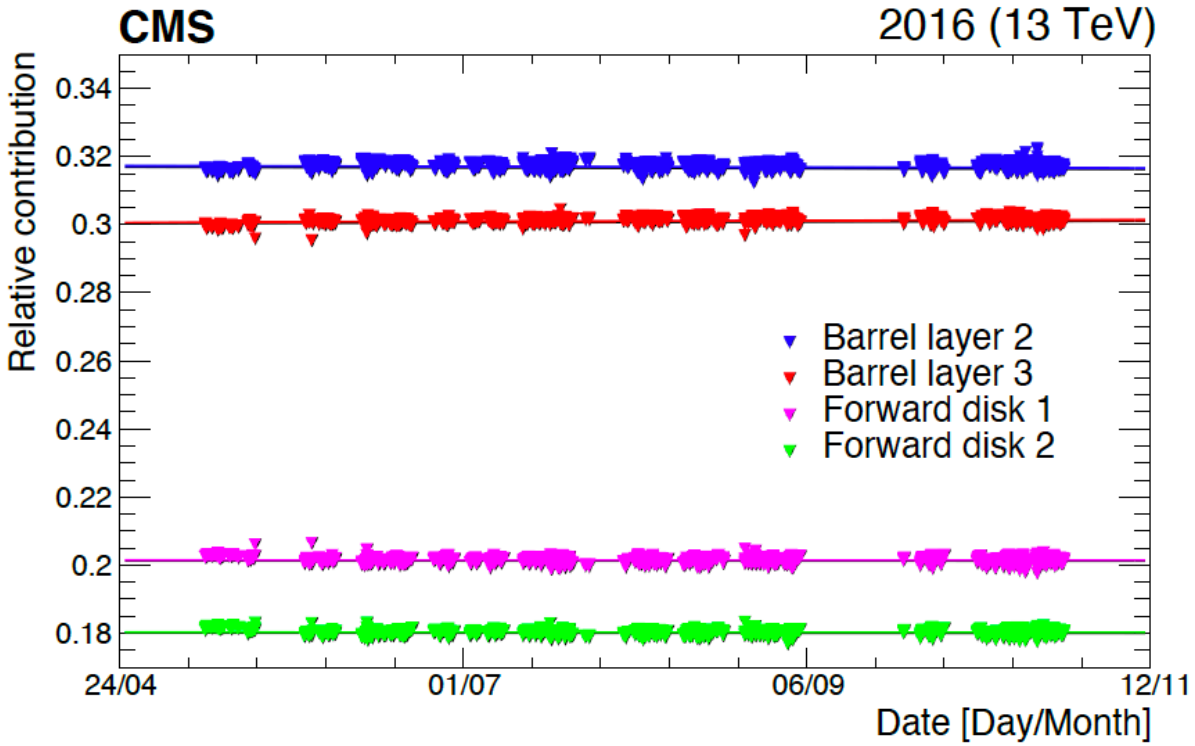

Figure 15: The relative contribution to the total number of observed pixel clusters from the four regions of the pixel detector used in the luminosity measurement (barrel layers 2 and 3, and inner and outer forward pixel disks), as a function of time throughout 2016. The lines represent first-order polynomial fits to the relative contributions from each region.

- Aa a function of integrated luminosity

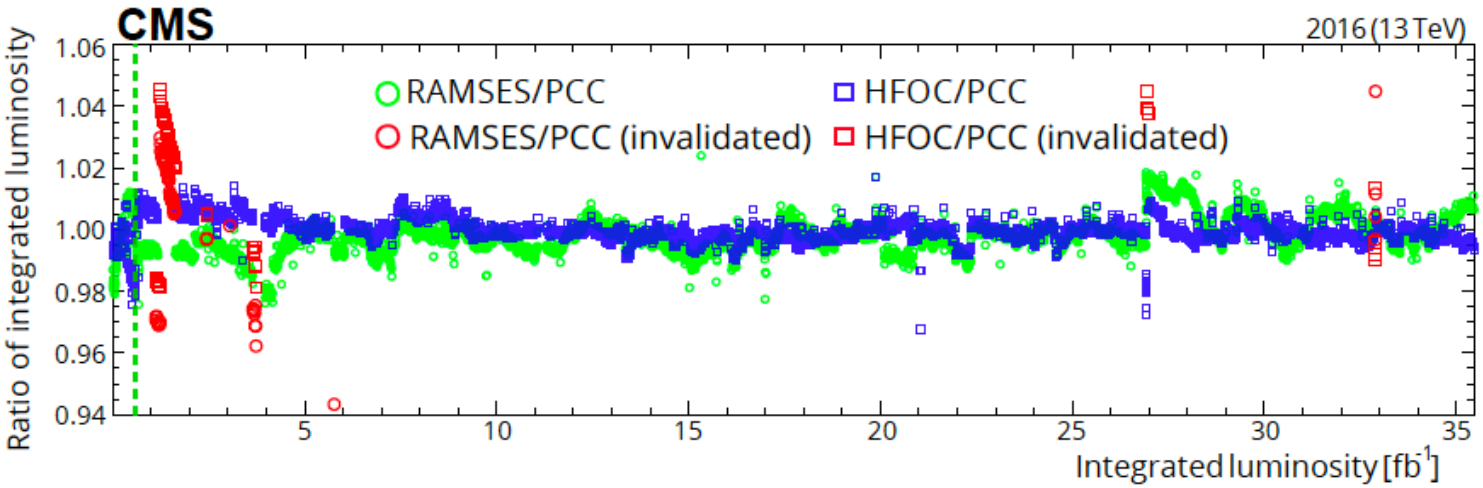

Figure 16: The luminosity measurements from PCC, HFOC, and RAMSES are compared as a function of the integrated luminosity in 2016. Comparison among three luminometers facilitates the identification of periods where a single luminometer suffers from transient stability issues. The ratios that are plotted in red contain invalidated data. The dashed line delineates the vdM calibration (fill 4954).

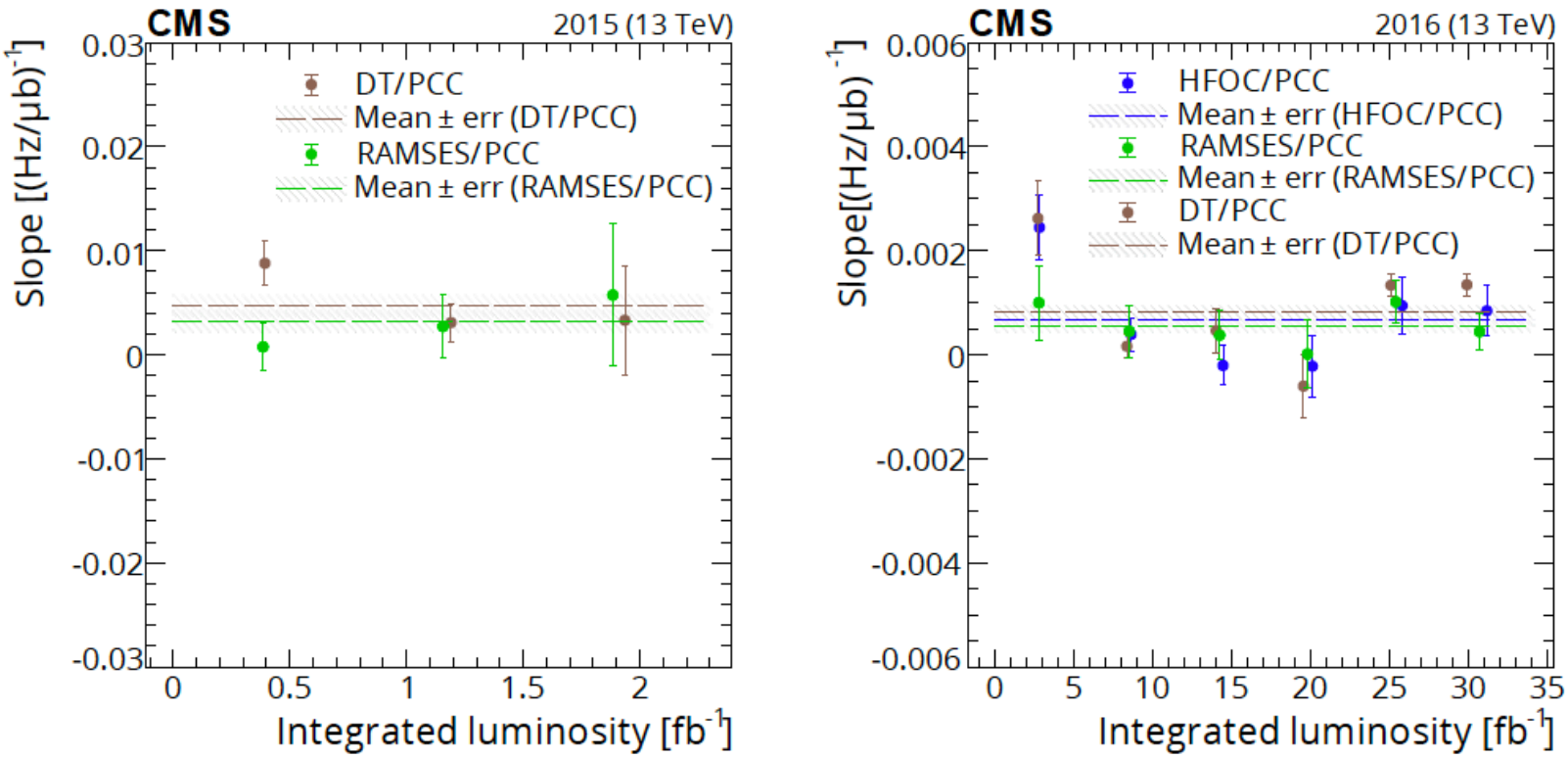

Figure 18: Linearity summary for 2015 (left) and 2016 (right) at $\sqrt{s} = 13\,\text{TeV}$. The slopes are plotted for each detector relative to PCC. The markers are averages of fill-by-fill slopes from fits binned in roughly equal fractions of the total integrated luminosity through the year. The error bars on the markers are the propagated statistical uncertainty from fitted slope parameters in each fill, which are weighted by integrated luminosities of each fill. The dashed lines and corresponding hatched areas show the average from the entire data set and its uncertainty.

Table 3: Summary of contributions to the relative systematic uncertainty in σ_{vis} (in %) at $\sqrt{s} = 13\,\text{TeV}$ in 2015 and 2016. The systematic uncertainty is divided into groups affecting the description of the vdM profile and the bunch population product measurement (normalization), and the measurement of the rate in physics running conditions (integration). The fourth column indicates whether the sources of uncertainty are correlated between the two calibrations at $\sqrt{s} = 13\,\text{TeV}$.

Source	2015 [%]	2016 [%]	Corr
Normalization uncertainty			
Bunch population			
Ghost and satellite charge	0.1	0.1	Yes
Beam current normalization	0.2	0.2	Yes
Beam position monitoring			
Orbit drift	0.2	0.1	No
Residual differences	0.8	0.5	Yes
Beam overlap description			
Beam-beam effects	0.5	0.5	Yes
Length scale calibration	0.2	0.3	Yes
Transverse factorizability	0.5	0.5	Yes
Result consistency			
Other variations in σ_{vis}	0.5	0.2	No
Integration uncertainty			
Out-of-time pileup corrections			
Type 1 corrections	0.3	0.3	Yes
Type 2 corrections	0.1	0.3	Yes
Detector performance			
Cross-detector stability	0.6	0.5	No
Linearity	0.5	0.3	Yes
Data acquisition			
CMS deadtime	0.5	$<$0.1	No
Total normalization uncertainty	1.2	1.0	—
Total integration uncertainty	1.0	0.7	—
Total uncertainty	1.6	1.2	—

How to obtain important results "luminosity independent" way ?

For example measure elastic and total xsections at the same time

optical theorem gives:

$$\sigma_{tot} = \frac{4\pi}{k}\,\mathrm{Im\ f(0)};$$

$where\ k - wave\ factor,$
$f(0) - forward\ elastic\ \ scattering\ amplitude$

hence

$$\sigma_{tot} = \frac{16\pi(\hbar c)^2}{1+\rho^2}\,\frac{d\sigma_{el}/_{dt}\,|_{t=0}}{\sigma_{tot}} \quad \rightarrow\rightarrow \quad \sigma_{tot} = \frac{16\pi(\hbar c)^2}{1+\rho^2}\,\frac{dN_{el}/_{dt}\,|_{t=0}}{N_{el}+N_{inel}}$$

where: $\rho = \frac{Ref(0)}{Imf(0)}$

The TOTEM Experiment / CMS TOTEM Collaboration

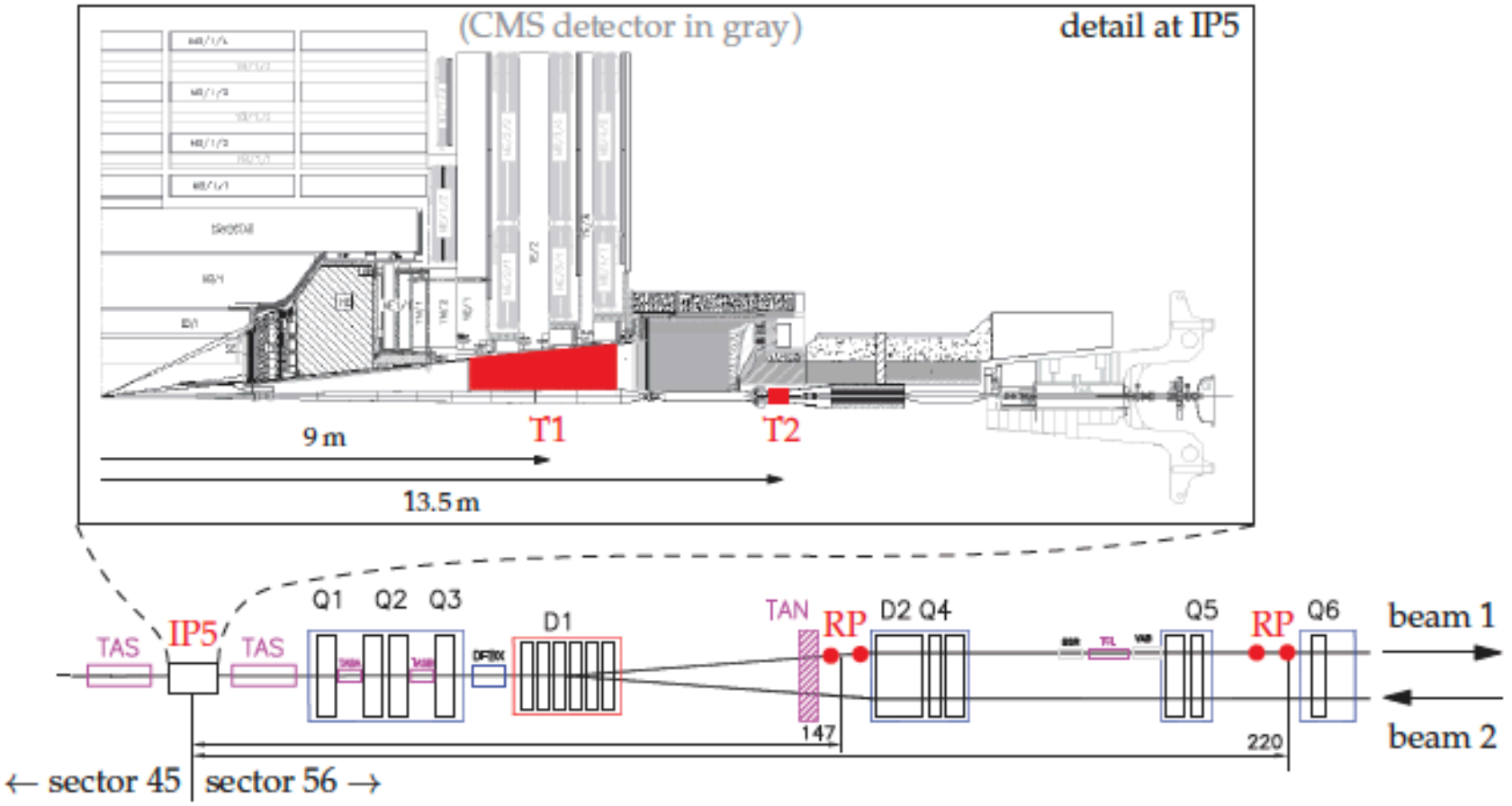

Fig. 1. A schematic view of the TOTEM detectors in the LHC.

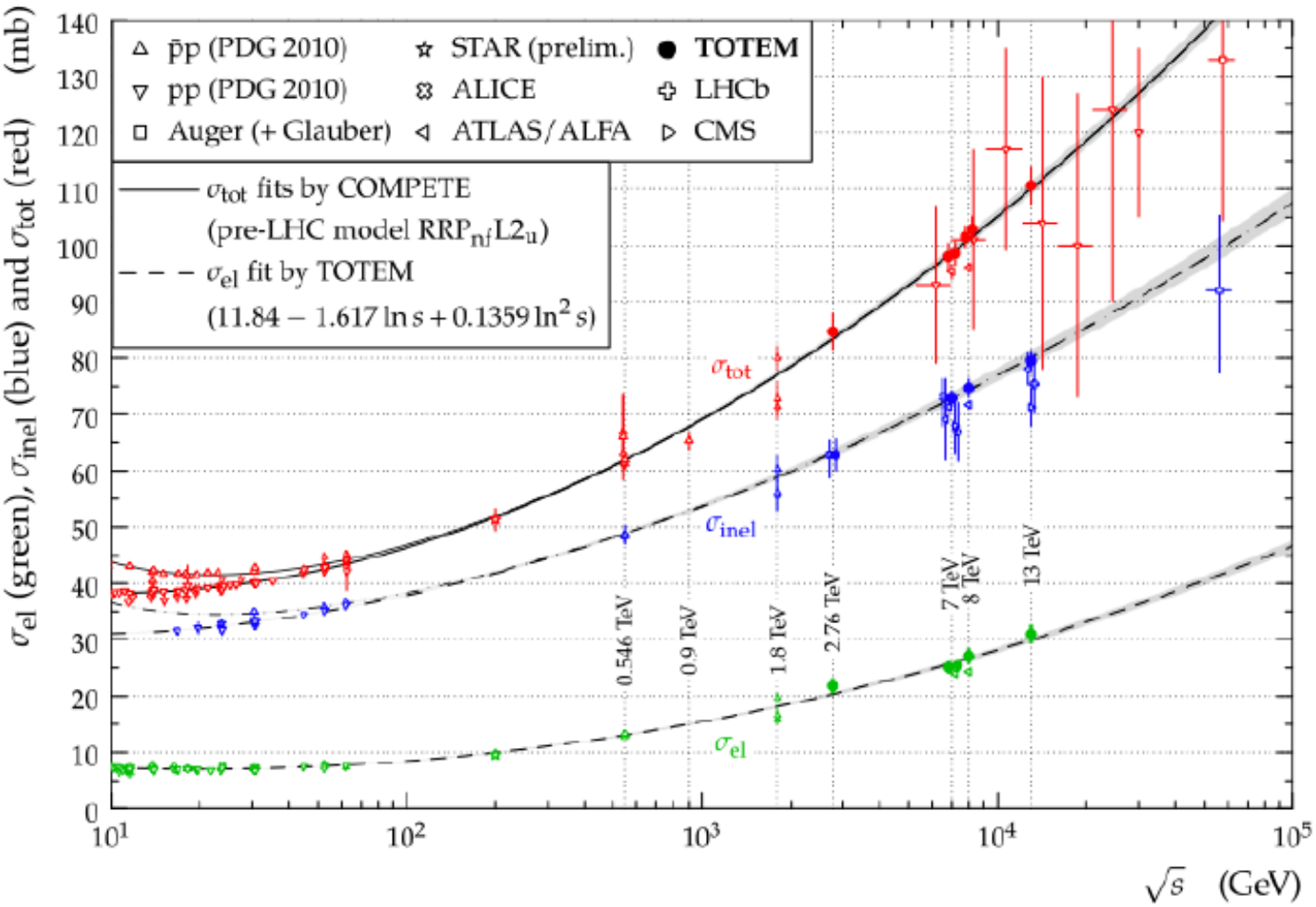

Fig. 4 Overview of elastic (σ_{el}), inelastic (σ_{inel}), total (σ_{tot}) cross section for pp and $p\bar{p}$ collisions as a function of $\sqrt{s}$, including TOTEM measurements over the whole energy range explored by the LHC [1–5,7,8,12–14,17,18,21,23,24,28,30,32]. Uncertainty band on theoretical models and/or fits are as described in the legend. The continuous black lines (lower for pp, upper for $p\bar{p}$) represent the best fits of the total cross section data by the COMPETE collaboration [26]. The dashed line results from a fit of the elastic cross section data. The dash-dotted lines refer to the inelastic cross section and are obtained as the difference between the continuous and dashed fits

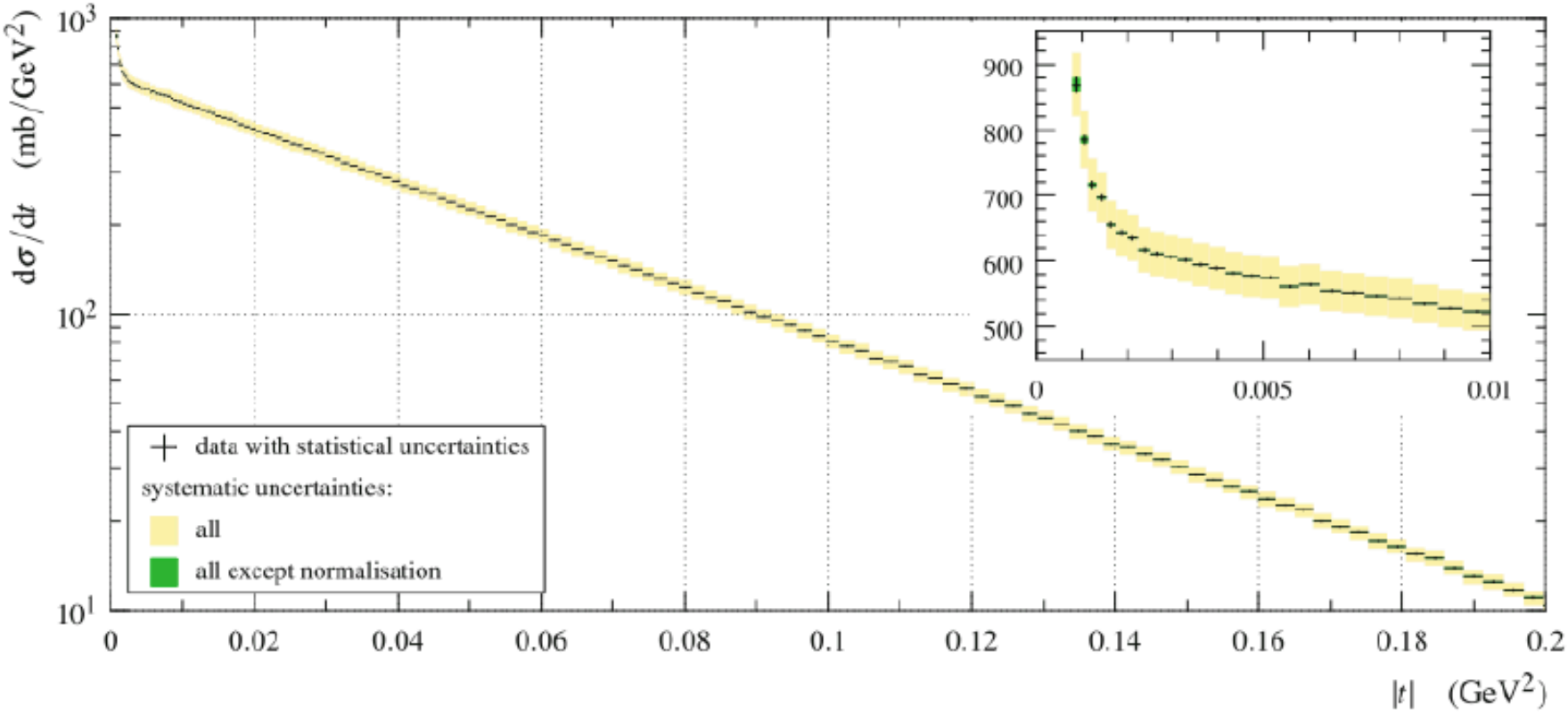

Fig. 10 Differential cross-section from Table 3 with statistical (bars) and systematic uncertainties (bands). The yellow band represents all systematic uncertainties, the green one all but normalisation. The bands are centred around the bin content. Inset: a low-$|t|$ zoom of cross-section rise due to the Coulomb interaction

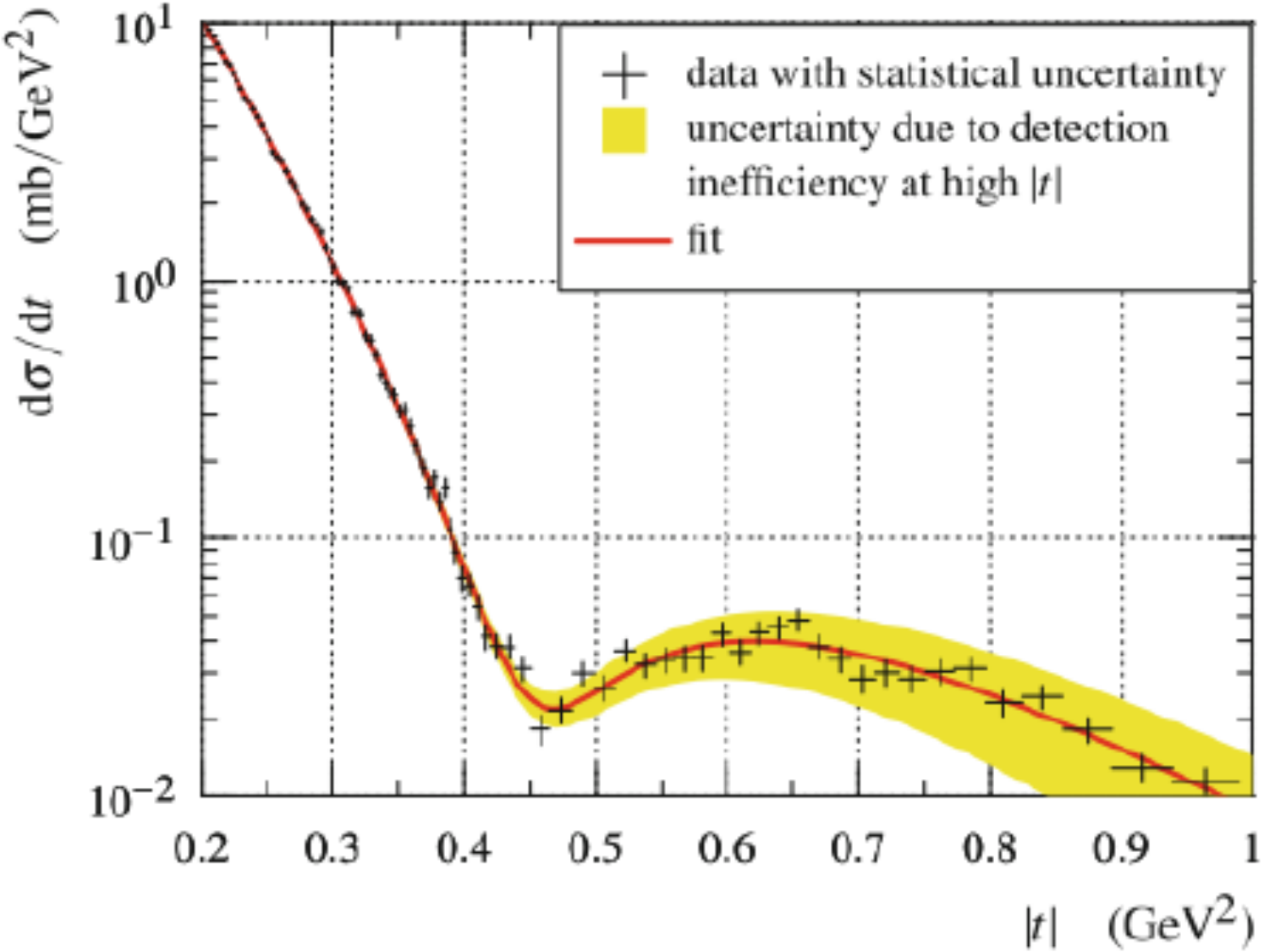
data with statistical uncertainty
uncertainty due to detection inefficiency at high |t|
fit
dσ/dt (mb/GeV²)
10¹
10⁰
10⁻¹
10⁻²
0.2
0.3
0.4
0.5
0.6
0.7
0.8
0.9
1
|t| (GeV²)

TOTEM Collaboration
Eur. Phys. J C 79 (2019) 785
CMS-TOTEM Collaboration
arXiv:2102.06945v1
TOTEM-D0 Collaboration
arXiv:2012.03981v2

$pp \rightarrow pp \; vs \; \overline{p}p \rightarrow \overline{p}p$

DISAGREEMNT!!!

explained by existence of the

ODERON

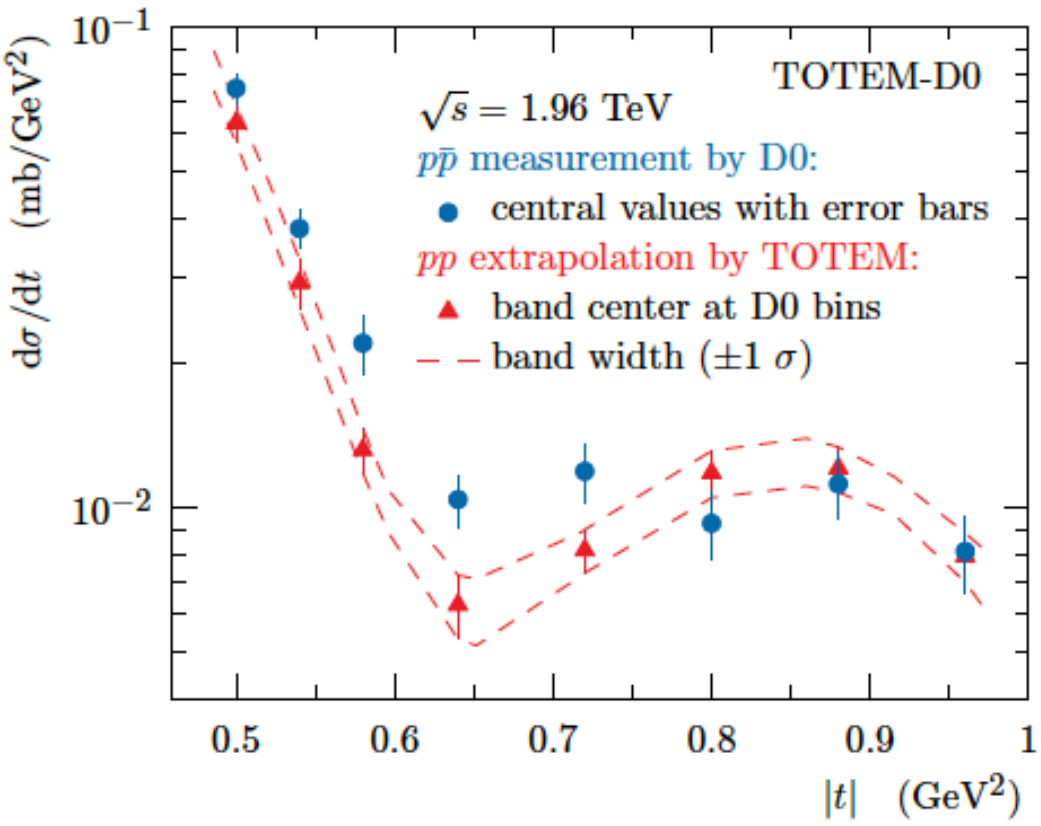

FIG. 4: Comparison between the D0 $p\bar{p}$ measurement at 1.96 TeV and the extrapolated TOTEM pp cross section, rescaled to match the OP of the D0 measurement. The dashed lines show the 1σ uncertainty band on the extrapolated pp cross section.

Odderon: well established in QCD

Odderon proposed in Regge phenomenology:
L. Lukaszuk, B. Nicolescu, Lett. Nuovo Cim. 8, 405 (1973)

Three Gluon Integral Equation and Odd c Singlet Regge Singularities in QCD
J. Kwiecinski, M. Praszalowicz, Phys.Lett.B 94 (1980) 413-416

A new Odderon intercept from QCD:
R. A. Janik, J. Wosiek, Phys. Rev. Lett. 82 (1999) 1092

Odderon in QCD:
J. Bartels, L.N. Lipatov, G. P. Vacca: Phys. Lett. B (2000) 178

Odderon in QCD with running coupling:
J. Bartels, C. Contreras, G. P. Vacca, *JHEP* 04 (2020) 183

For an excellent theory intro/review, see Yu. Kovchegov's CTEQ Webinar, April 28, 2021
http://youtu.be/yHBO3zcB3V4

The BKP Equation

Bartels (1980), Kwiecinski&Prasza

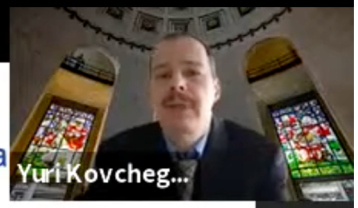

The BFKL equation describes evolution of the 2-reggeized gluon system shown below (a *C*-even exchange)

The BKP equation describes evolution of an n-reggeized gluon system. For 3 reggeized gluons in d^{abc} color state it gives a *C*-odd exchange.

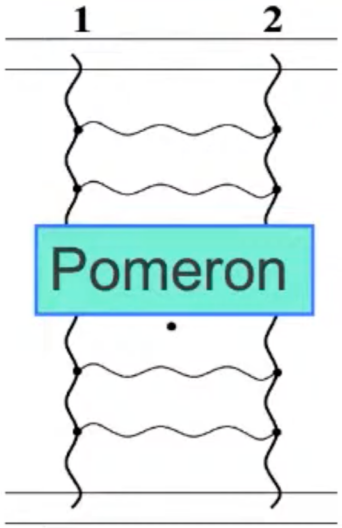

$$Y = \ln(s/\perp^2)$$

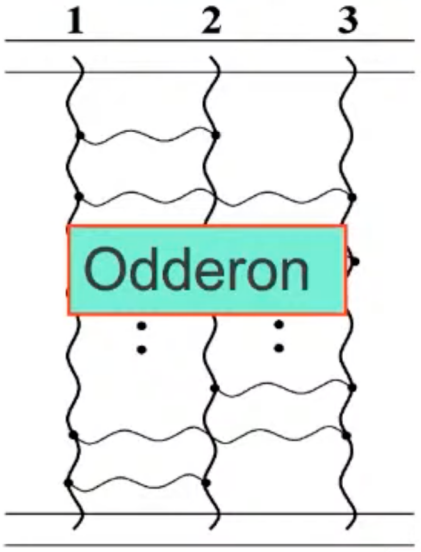

Jan Kwiecinski 1938 - 2003

Absolutely the kindest man I have ever met in my whole life.
CERN Course: Jan-Feb 2004

$$\frac{\partial f}{\partial Y} = K_{12} \otimes f$$

$$\frac{\partial O}{\partial Y} = K_{12} \otimes O + K_{23} \otimes O + K_{31} \otimes O$$

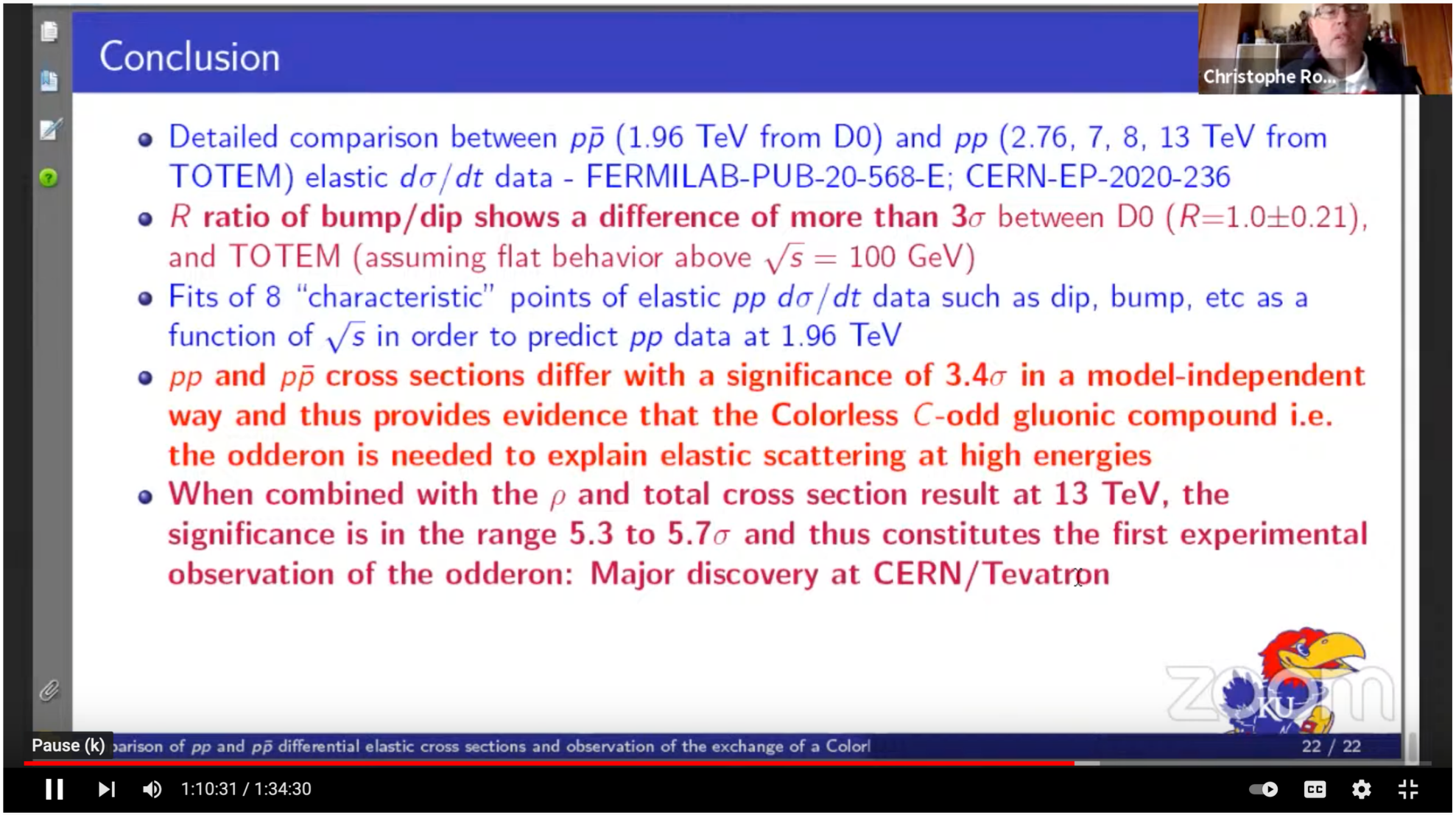

CTEQ Webinar: The Discovery of the Odderon: from Theory to the Experimental Results by TOTEM/D0

A.Breakstone et al., Phys. Rev. Lett. 54,2180 (1985)

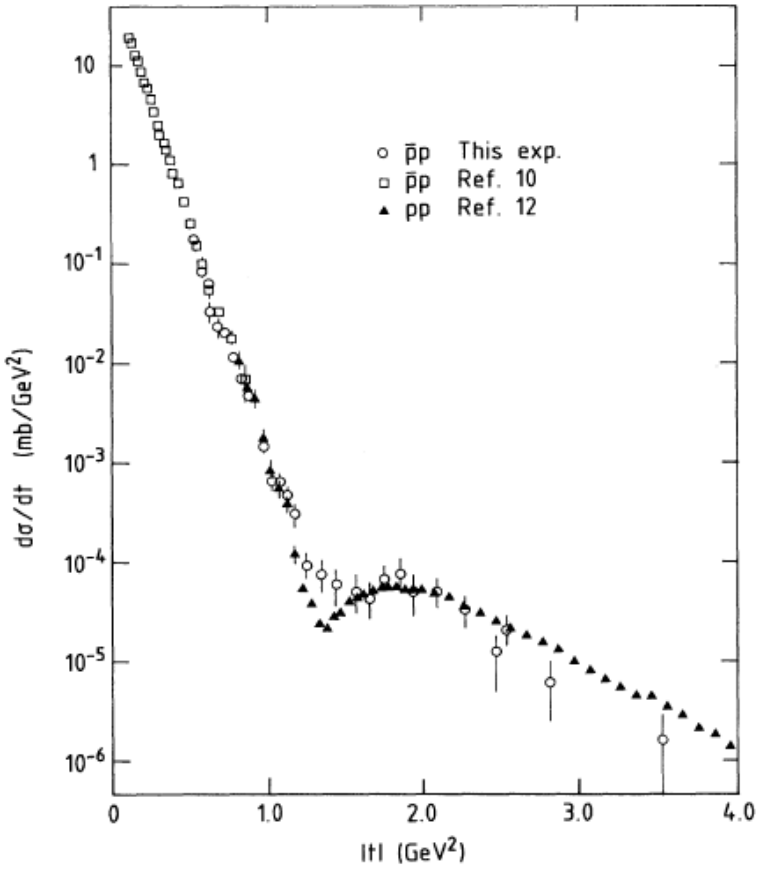

FIG. 2. Elastic differential $\bar{p}p$ cross section at $\sqrt{s} = 53$ GeV. Only t-dependent errors are shown. The systematic scale error is estimated at $\pm 30\%$. Included are the low-t data from our previous experiment (Ref. 10) and the pp data of Ref. 12.

ISR/SFM Data

For more information see Review:
P.Grafstrom W.Kozanecki. Luminosity determination at proton colliders,
Progers in Particle and Nuclear Physics 81 (2015) 97-148

Thank you for your patience !

Backup

Luminosity
with
precision 1.7%

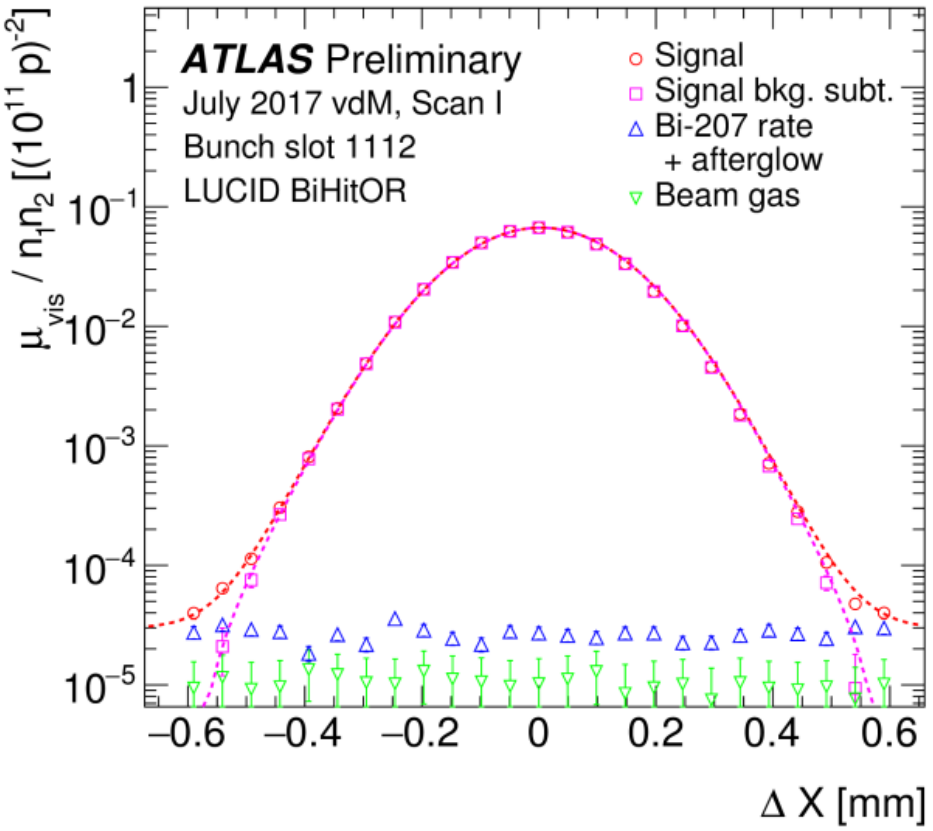

With vdM method strategy is the following:

- Make scanning to measure $\mathcal{L}_b$
- Knowing $\mathcal{L}_b$ and rate ($< N_{observables} >$)at given luminometer find σ_{vis} for this luminometer

$$\mathcal{L}_b = \frac{< N_{observables} >}{< N_{observables/interaction} >} * \frac{\nu_r}{\sigma} = < N_{observables} > \frac{\nu_r}{\sigma_{vis}}$$

$$\sigma_{vis} = \frac{< N_{observables} > \nu_r}{\mathcal{L}_b}$$

↑ *this is our calibration value taken at vdM scan luminosity*

it's error will define accuracy for future luminosity measurements

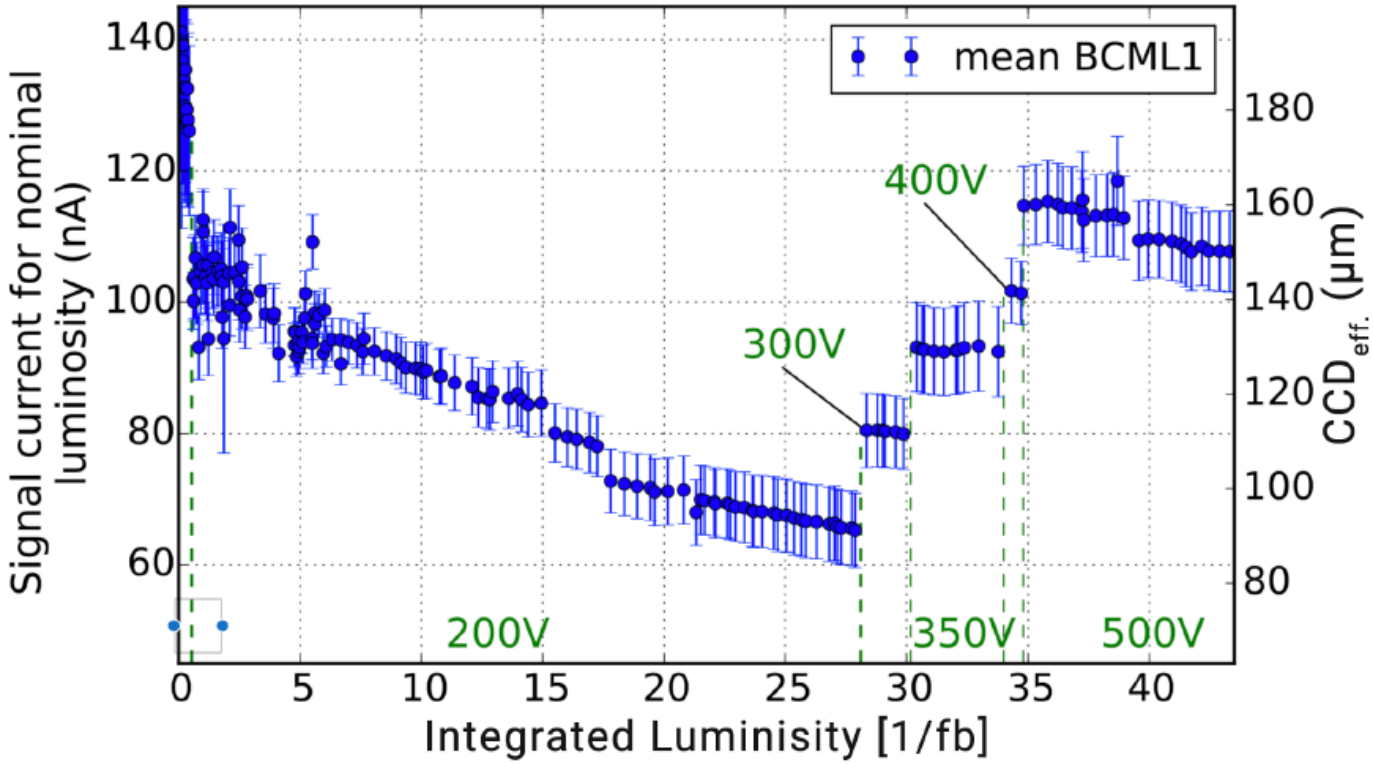

Figure 4.5: BCML1 signal degradation during the first part of Run 2 (2015–2016) as a function of integrated luminosity delivered. The dashed vertical lines indicate times when the bias voltage was changed. During the first 0.5 fb^{-1} in Run 2, the BCML1 detector was operated at 500 V. However, due to problems with the CMS magnet, the BCML1 bias voltage was reduced to 200 V. At 200 V, the signal efficiency dropped to 50%, after which it was increased to 88% by increasing the HV up to 500 V. Plot from Ref. [86].

2.2 Summary on luminosity precision goals

As was shown, the luminosity uncertainty becomes subleading for most precision SM analyses when it is smaller than ≈1%, i.e., comparable to the uncertainties in trigger and offline selection and reconstruction efficiencies. Some measurements, such as those of inclusive Drell–Yan production, would benefit from an even higher luminosity precision, and they could be carried out on a subset of the expected data set, which could be selected for improved luminosity precision based on detector data quality. These measurements provide a strong motivation for achieving an uncertainty in the integrated luminosity even at the sub-percent level.

Recently, projections have assumed the relative uncertainty in the integrated luminosity at the HL-LHC to be 1.0% [25].

Table 12
Example breakdowns of the fractional systematic uncertainties affecting the determination of the visible *pp* cross-section σ_{vis} by the *vdM* method at the LHC. Blank entries correspond to cases where the uncertainty is either not applicable to that particular experiment or scan session, is considered negligible by the authors, or is not mentioned in the listed reference. In some cases, uncertainties quoted separately in the original publication have been regrouped to fit in a common classification.

Experiment	ALICE	ATLAS	CMS	LHCb
Reference	[118]	[26]	[133]	[127]
pp running period	2011	2011	2012	2012
$\sqrt{s}$ (TeV)	2.76	7.0	8.0	8.0
Total beam intensity	0.34%	0.23%	0.3%	0.23%
Bunch-to-bunch fraction	0.08%	0.20%	–	0.10%
Ghost charge and satellite bunches	0.45%	0.44%	0.2%	0.23%
Subtotal, bunch-population product	0.57%	0.54%	0.4%	0.34%
Orbit drift & beam-position jitter	–	0.32%	0.1%	0.32%
Bunch-to-bunch σ_{vis} consistency	–	0.55%	–	–
Emittance growth & scan-to-scan reproducibility	0.64%	0.67%	0.2%	0.80%
Dynamic β & beam–beam deflections	0.40%	0.50%	0.7%	0.28%
vdM fit model	–	0.28%	2.0%	0.54%
Non-factorization effects	0.60%	0.50%	in fit model	0.80%
Subtraction of luminosity backgrounds	0.30%	0.31%	–	0.14%
Subtotal, beam conditions	1.01%	1.24%	2.2%	1.33%
Difference of reference $\mathcal{L}_{spec}$ across luminometers	–	0.29%	–	–
μ-dependent non-linearities during *vdM* scans	–	0.50%	–	–
Other instrumental effects	0.20%	–	–	0.09%
Statistical uncertainty	–	0.04%	0.5%	0.04%
Subtotal, instrumental effects	0.20%	0.58%	0.5%	0.10%
Absolute beam-separation scale	1.41%	0.42%	0.5%	0.50%
Total systematic uncertainty on σ_{vis}	1.84%	1.53%	2.3%	1.47%

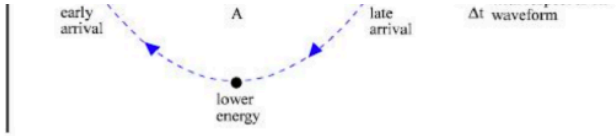

As we said above, **particle A is called the synchronous particle.** All the other particles, like **particle B, will oscillate longitudinally around A** under the influence of the RF system. These oscillations are called synchrotron oscillations.

For larger energy deviations these circles get flattened into ellipses, as the restoring force drops off from the linear central valves.

The Bucket area is called **longitudinal acceptance** and has unites of energy x time (eV·s)

The Bunch area is called **longitudinal emittance** and it has also unites of energy x time (eV·s)

Bunch area (ellipse) = $\pi \cdot a \cdot b \rightarrow$ Area = $\pi \cdot (\Delta E/2) \cdot (\Delta t/2)$

So, the **Longitudinal Emittance** = $\pi \cdot \Delta E \cdot \Delta t/4$

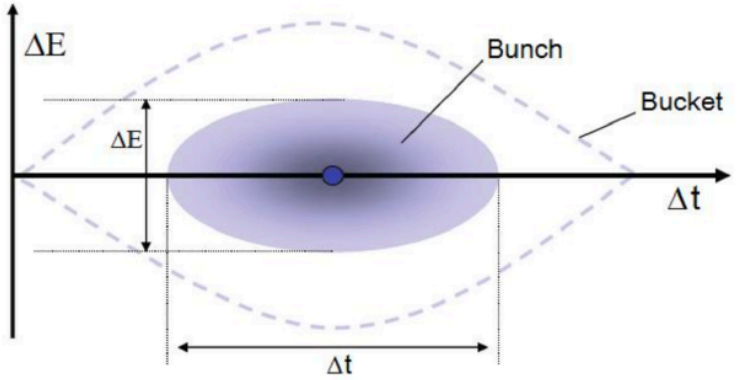

The LHC longitudinal acceptance (Bucket area) at 7 TeV is **7.91 eVs**

Longitudinal Emittance for LHC is **2.5 eVs** for top energy

For more details see **Baird S. (2007).** *"ACCELERATORS FOR PEDESTRIANS"*, AB-Note-2007-014 OP, CERN February 2007

The RF Cavities generate a longitudinal oscillanting voltage, which is applied across an isolated gap in the vacuum chamber, so that the particle sees an accelerating voltage at the gap, and the voltage then cancels out as the particle goes around the rest of the machine. However **we must make sure that the particle always sees an accelerating voltage at the gap, so the RF frequency must always be an integer multiple (h) of the revolution frequency.**

$$f_{RF} = h \cdot f_{rev}$$

where **h** is known as the **harmonic number**.

A particle with a speed v = βc circulates around the machine with a period or frecuency:

$$T_{rev} = 2\pi R/\beta c \quad \text{or} \quad f_{rev} = \beta c/2\pi R$$

In LHC h is very large.

RF cavities frecuency is 400 MHz, the speed of protons is βc ~c , 2πR = 26659 m.

So, we have;

$$\text{Harmonic Number:} \quad h = f_{RF}/f_{rev}$$

$$h = (400 \cdot 10^6)/(c/26659)$$

$$\text{Harmonic Number} \approx 35640$$

The segments of the circumference centred on these points are called **BUCKETS**.

A particle exactly synchronised with the RF frequency is called **synchronous particle**. As we will see below, **all the other particles in the accelerator will oscillate longitudinally around the synchronous particles** under the influence of the RF system. This means that instead of being spread uniformly around the circumference of the accelerator **the particles get "clumped" around the synchronous particle in a BUNCH**. This bunch is contained in an RF bucket.

So, LHC might accelerate a beam made up of 35640 bunches.

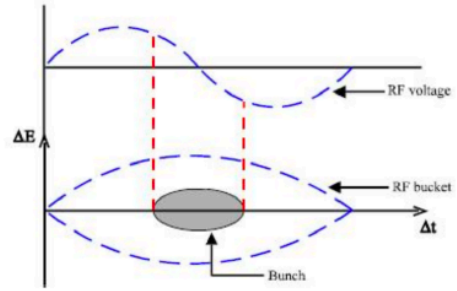

It is **important to note** that two synchrotrons are included in LHC injection chain: PS and SPS. In fact PS is responsible for providing the bunch packets with 25 ns spacing that finally will be injected from SPS in the LHC.

Emittance can be defined as the smallest opening you can squeeze the beam through, and can also be considered as a measurement of the parallelism of a beam.
It has units of length, but is usually referred to as "length x angle", for example, "millimeter x milli-radians". It can be measured in all three spatial dimensions. The dimension parallel to the motion of the particle is called the **longitudinal emittance**. The other two dimensions are referred to as the **transverse emittances**.

The amplitude function, ***β*** *,* is determined by the accelerator magnet configuration (basically, the quadrupole magnet arrangement) and powering. When expressed in terms of **σ** (cross-sectional size of the bunch) and the transverse emittance, the ***amplitude function β*** **becomes**(see here)**:**

$$\beta = \pi \cdot \sigma^2 / \varepsilon \quad (1)$$

So, **Beta is roughly the width of the beam squared divided by the emittance.** If **Beta is low, the beam is narrower, "squeezed". If Beta is high, the beam is wide and straight.**
Beta has units of length.
Sometimes **Beta** is referred as the distance from the focus point that the beam width is twice as wide as the focus point.

Improved Bhabha cross section at LEP and the number of light neutrino species ☆

Patrick Janot [a,*], Stanisław Jadach [b]

[a] CERN, EP Department, 1 Esplanade des Particules, CH-1217 Meyrin, Switzerland
[b] Institute of Nuclear Physics PAN, ul. Radzikowskiego 152, 31-342 Kraków, Poland

ARTICLE INFO

Article history:
Received 17 December 2019
Received in revised form 13 February 2020
Accepted 19 February 2020
Available online 25 February 2020
Editor: L. Rolandi

ABSTRACT

In e^+e^- collisions, the integrated luminosity is generally measured from the rate of low-angle Bhabha interactions $e^+e^- \to e^+e^-$. In the published LEP results, the inferred theoretical uncertainty of $\pm 0.061\%$ on the predicted rate is significantly larger than the reported experimental uncertainties. We present an updated and more accurate prediction of the Bhabha cross section in this letter, which is found to reduce the Bhabha cross section by about 0.048%, and its uncertainty to $\pm 0.037\%$. When accounted for, these changes modify the number of light neutrino species (and its accuracy), as determined from the LEP measurement of the hadronic cross section at the Z peak, to $N_\nu = 2.9963 \pm 0.0074$. The 20-years-old 2σ tension with the Standard Model is gone.

Table 3
Inspired from Refs. [28,29,25]: Summary of the theoretical uncertainties for a typical LEP luminosity detector covering the angular range from 58 to 110 mrad (first generation) or from 30 to 50 mrad (second generation). The total uncertainty is the quadratic sum of the individual components.

LEP Publication in:	1994		2000		2019	
LumiCal generation	1st	2nd	1st	2nd	1st	2nd
Photonic $\mathcal{O}(\alpha^2 L_e)$	0.15%	0.15%	0.027%	0.027%	0.027%	0.027%
Photonic $\mathcal{O}(\alpha^3 L_e^3)$	0.09%	0.09%	0.015%	0.015%	0.015%	0.015%
Z exchange	0.11%	0.03%	0.09%	0.015%	0.090%	0.015%
Vacuum polarization	0.10%	0.05%	0.08%	0.040%	0.015%	0.009%
Fermion pairs	0.05%	0.04%	0.05%	0.040%	0.010%	0.010%
Total	0.25%	0.16%	0.13%	0.061%	0.100%	0.037%

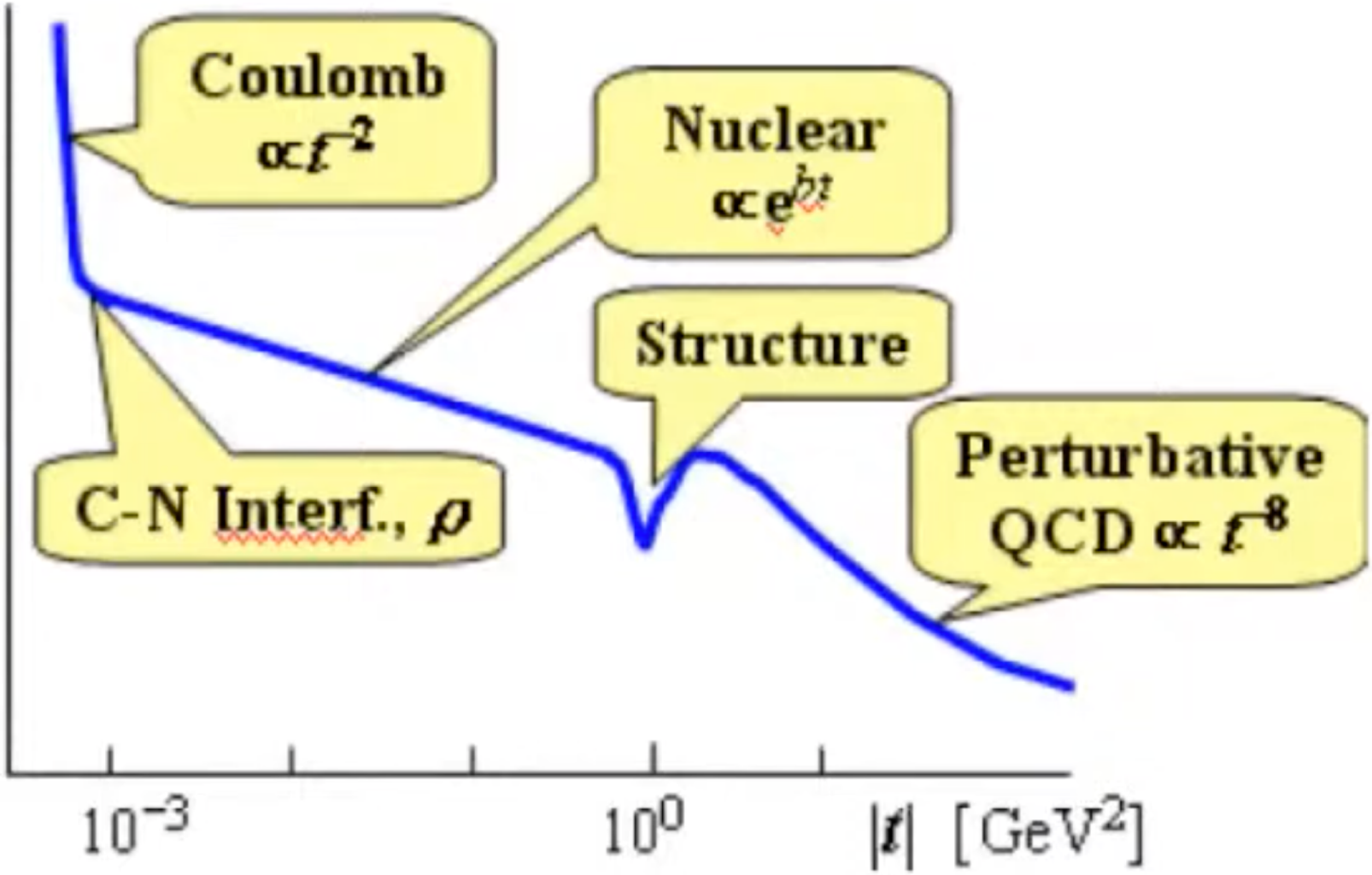
Coulomb
$\propto t^{-2}$
Nuclear
$\propto e^{bt}$
Structure
C-N Interf., ρ
Perturbative
QCD $\propto t^{-8}$
10^{-3}
10^{0}
$|t|$ [GeV^2]

From Wikipedia….

Odderon

The **odderon**, the counterpart of the pomeron that carries odd charge parity was introduced in 1973 by Leszek Łukaszuk and Basarab Nicolescu.[2] Odderons exist in QCD as a compound state of three reggeized gluons.[3] Potentially theorized in 2015.[4]It was potentially observed only in 2017 by the TOTEM experiment at the LHC.[3] This observation was later confirmed in a joint analysis with the DØ experiment at the Tevatron and appeared in the media as the particle's discovery in March 2021.[5][6][7][8][9][10]

ities in the complex angular momentum plane. The simplest examples, Regge poles, lead to terms of the form $\eta f(t)(s/s_0)^{\alpha(t)}$, where t is the four-momentum transferred squared, η the "signature" with value ± 1, and $\alpha(t)$ the "trajectory" of the particular Regge pole. Positive signature poles give the same (positive) contribution to both pp and $p\bar{p}$ scattering. Negative signature poles give opposite sign contributions to pp and $p\bar{p}$ scattering. Using the optical theorem, each such Regge pole contributes a term proportional to $s^{\alpha(0)-1}$ to the total cross section. The largest contributor at very high energy, called the Pomeron, is the positive signature Regge pole whose $\alpha(0)$ is the largest. To explain the rising total cross section, the Pomeron should have $\alpha(0)$ just larger than one. A $\eta = -1$ Regge exchange with a similarly large $\alpha(0)$, called the odderon [7, 8] was recognized as a possibility but was initially not well motivated theoreti-

Table 2: Summary of the BCID-averaged corrections to σ_{vis} (in %) obtained with the vdM scan calibrations at $\sqrt{s} = 13$ TeV in 2015 and 2016. When a range is shown, it is because of possible scan-to-scan variations. To obtain the impact on σ_{vis}, each correction is consecutively included, the fits are redone following the order below, and the result is compared with the baseline. The impact from transverse factorizability is obtained separately (as discussed in Section 4.4).

Source	Impact on σ_{vis} [%]	
	2015	2016
Ghost and satellite charge	+0.2	+0.3
Orbit drift	+0.6 to +1.0	+0.2 to +1.0
Residual beam position corrections	−0.6 to +0.4	−0.5 to −0.2
Beam-beam effects	+0.6	+0.4
Length scale calibration	−0.4	−1.3
Transverse factorizability	+0.8 to +1.3	+0.6

Luminous region evolution (3 dim.)

The bunch profiles $\rho_j(x,y,z)$, parameterized per beam j, are the sum of three individual Gaussian distributions $g_{j,1\ldots3}(x,y,z)$ with common mean, but arbitrary width and orientation parameters (referred to as "bunch parameters" in the following):

$$\rho_j(x,y,z) = w_{j,1}g_{j,1}(x,y,z) + w_{j,2}g_{j,2}(x,y,z) + (1 - w_{j,1} - w_{j,2})g_{j,3}(x,y,z). \quad (23)$$

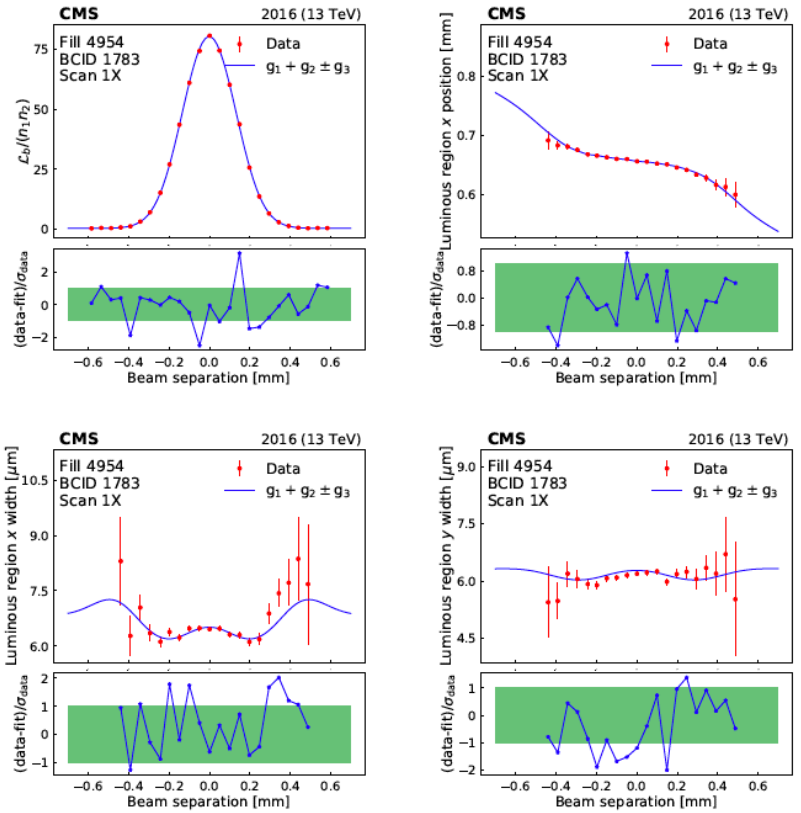

Figure 12: Beam-separation dependence of the luminosity and some luminous region parameters during the first horizontal vdM scan in fill 4954. The points represent the luminosity normalized by the beam current product (upper left), the horizontal position of the luminous centroid (upper right), and the horizontal and vertical luminous region widths (lower left and right). The error bars represent the statistical uncertainty in the luminosity, and the fit uncertainty in the luminous region parameters. The line is the result of the three-Gaussian ($g_1 + g_2 \pm g_3$) fit described in the text. In all cases, the lower panels show the one-dimensional pull distributions.